Theses and Dissertations

7-2015

Paleoclimate Implications from Stable Isotope Analysis of Sedimentary Organic Carbon and Vertebrate Fossils from the Cedar Mountain Formation, UT, U.S.A.

Garrett Andrew Hatzell
University of Arkansas, Fayetteville

Follow this and additional works at: http://scholarworks.uark.edu/etd

Part of the Geology Commons, Paleobiology Commons, and the Paleontology Commons

Paleoclimate Implications from Stable Isotope Analysis of Sedimentary Organic Carbon and Vertebrate Fossils from the Cedar Mountain Formation, UT, U.S.A.

Paleoclimate Implications from Stable Isotope Analysis of Sedimentary Organic Carbon and Vertebrate Fossils from the Cedar Mountain Formation, UT, U.S.A.

A thesis submitted in partial fulfillment
of the requirements for the degree of
Master of Science in Geology

by

Garrett A. Hatzell
University of Arkansas
Bachelor of Science in Geology, 2011

July 2015
University of Arkansas

This thesis is approved for recommendation to the Graduate Council.

_____
Dr. Celina A. Suarez
Thesis Director

_____   _____
Dr. Phillip D. Hays   Dr. Gregory Dumond
Committee Member   Committee Member

Abstract

Oxygen and carbon isotopic compositions of fossilized vertebrate teeth and bone were analyzed to determine isotopic values of vertebrate faunal diet from the early Cretaceous Cedar Mountain Formation of Utah. Results for $\delta^{18}O$ of PO_4 ($\delta^{18}O_p$) (Suarez et al., 2014) from the same data set have been compared to the $\delta^{18}O$ of CO_3 ($\delta^{18}O_c$) portion of teeth and turtle shell to determine if diagenetic alteration of the isotopes has occurred by plotting the line of best fit equation that models the relationship between unaltered $\delta^{18}O_P$ and $\delta^{18}O_C$ of modern mammals from Iacumin et al., 1996. Results indicate slight diagenesis of some specimens has occurred.

Mean annual precipitation (MAP) estimates, using the equations from Kohn (2010) and Diefendorf et al., (2010), were determined for each sampled stratigraphic member using carbon isotopic values derived from vertebrate faunal diet estimations from bioapatite, based on the observation that $\delta^{13}C$ of modern C3 plants increases with decreasing MAP (Kohn, 2010; and others). Values indicate a prolonged period of semi-arid to arid climate in the Ruby Ranch and Yellow Cat members of the CMF likely caused by a rain-shadow (Suarez et al., 2014) on the eastern, leeward side of the uplifting Sevier Fold and Thrust belt (SFTB). The upper Mussentuchit Member becomes much more humid as the Western Interior foreland basin, continues to subside, eventually becoming inundated by the Western Interior Seaway.

The basal Cretaceous CMF sits unconformably atop the Late Jurassic Morrison Formation, with a hiatus of ~20 Ma (Kirkland and Madsen, 2006). Chemostratigraphic curves of the basal Yellow Cat member (YCM) were constructed using $\delta^{13}C$ of bulk organics of sediment, and $\delta^{13}C$ and $\delta^{18}O$ of inorganic carbonate of sediment in an attempt to correlate with the early Cretaceous chemostratigraphic record. Correlating positive and negative carbon isotope excursions (PCIEs and NCIEs) from the YCM to stratigraphically well-constrained marine sections lends evidence

for an age determination of the basal CMF. Correlations indicate the YCM to be Barremian to Aptian (~130-120 Ma) in age and detect several distinct CIEs of this period, specifically the B5-B8 excursions of the Barremian and the A1-C5 excursions of the Aptian.

Acknowledgments

Thank you to Celina Suarez for funding this study and supplying the vertebrate samples to make this paper possible. Thank you to Lyndsey Conaway and Erik Pollack for assisting in running of samples in the University of Arkansas Stable Isotopes Laboratory. Thank you to Marina Suarez, Jim Kirkland, and Aisha Al-Suwaidi for help with field work and data analysis.

Dedication

Dedicated to my parents, Frank and Joyce Williams; and friends and family I have lost: James Wetherington, Britton Redifer, Bob Hatzell, and Boyd Hatzell.

Table of Contents

List of Figures

I. Introduction

Utah has long been world famous for its dinosaur fossil record. The Late Jurassic Morrison Formation yields abundant fossil sites such as the Carnegie Quarry at Dinosaur National Monument and the Cleveland-Lloyd Dinosaur Quarry. The Kaiparowits Formation in Grand Staircase-Escalante National Monument preserves one of the most complete Late Cretaceous sections and dinosaur fossil records in the world (Kirkland et al., 1999). More recently, the richness of the Early Cretaceous dinosaur fossil record has been observed in the layers of the Cedar Mountain Formation (CMF). The CMF of east-central Utah offers a diverse assemblage of lower Cretaceous terrestrial vertebrate fauna and records a large time span of fluctuating climatic conditions (Kirkland et al., 1999).

The rising Sevier Mountains provided sediments to the CMF and likely influenced regional climate and precipitation patterns of the area (Suarez et al., 2014), as mountain ranges do today. Isotopic compositions of unaltered fossilized bioapatite from the CMF should preserve values that can be used to decipher past precipitation rates and isotopic compositions, paleoelevation, and paleoclimates, as other oxygen isotope analyses have done (e.g., Koch, 1998; Kohn and Cerling, 2002; Ufnar et al., 2004; Kohn and Dettman, 2007; Fricke et al., 2008, 2009; Suarez et al., 2009; Suarez et al., 2012, 2014). One objective of this study is to observe the regional effects of mountain building on precipitation rates using terrestrial faunal remains. Vertebrate bioapatite samples were analyzed by Suarez et al., (2014) for $\delta^{18}O$ of hydroxylapatite PO_4, this study has analyzed the $\delta^{18}O$ of hydroxylapatite CO_3 from the same sample set in an effort to detect possible diagenetic alteration of $\delta^{18}O$. The $\delta^{13}C$ of the CO_3 portion of herbivorous vertebrate remains has been analyzed to estimate $\delta^{13}C$ of diet (C3 plants) to infer mean annual paleoprecipitation (MAP) rates for each of the sampled depositional members, based on

1

calculations described by Kohn (2010) and Diefendorf et al., (2010) in an effort to observe how

ongoing orogenesis affected the climate of the CMF depositional area through time.

The CMF was deposited at a time in Earth's history that experienced significant global

climate perturbations in the form of carbon isotope excursions (CIEs) and oceanic anoxic events

(OAEs) with major extinctions likely arising from these disturbances (Ludvigson et al., 2010a).

These global climatic disturbances are well documented in marine records and can be recognized

and characterized within the terrestrial record (Grocke et al., 1999; Jenkyns, 2003; Ludvigson et

al., 2010a). CIEs are indicated by the presence of temporally correlated stratigraphic sections

from different parts of the world that display very similar $\delta^{13}C$ chemostratigraphic trends

(Saltzman and Thomas, 2012). Recognition of these spatially varying, distinct $\delta^{13}C$

chemostratigraphic trends allows for recognition of a global CIE, of which several are

documented throughout the Cretaceous Period. Another aspect of this study is to

chemostratigraphically correlate C-isotope curves of the basal CMF with C-isotope curves of

well dated Cretaceous marine sections in an effort to generate a relative age date for the oldest

Cretaceous rocks of Utah.

II.   Geologic Setting and Background

A.   Stratigraphy and Paleontology

The early Cretaceous Cedar Mountain Formation outcrops (Fig. 1.) in east-central Utah, north

of Moab and Arches National Park, in the San Rafael Swell, and the Uinta basin of north-east

Utah (not a focus area of this study). First designated by Stokes (1949), the CMF was described

as a drab mudstone between the Jurassic Morrison Formation and the middle Cretaceous Dakota

Formation (Fig. 2.), but since then the boundaries of the CMF have been expanded to include

much of what was originally designated as upper Jurassic Morrison (Suarez et al., 2014). Based
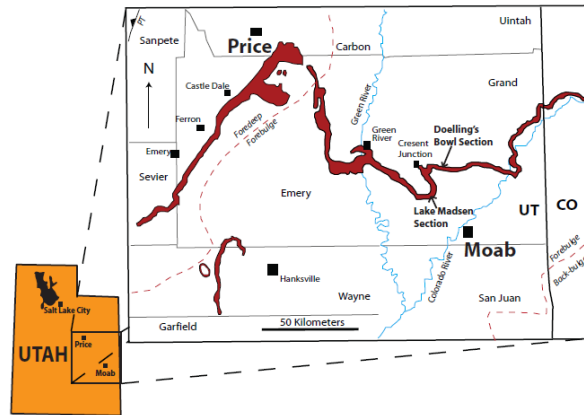
Figure 1. Outcrop map of CMF exposures in eastern Utah (Modified from Suarez et al., 2014). Foredeep, forebulge, and back bulge boundaries during Pavant thrust event depicted, with thrust boundary in northwest corner.

on the distribution of distinct dinosaur faunas and their relationships to specific rock types, the

CMF has been divided into 5 informally recognized depositional members. In ascending order,

they are the Buckhorn Conglomerate, the Yellow Cat Member (YCM), the Poison Strip

Sandstone (PSS), the Ruby Ranch Member (RRM), and the Mussentuchit Member (MM).
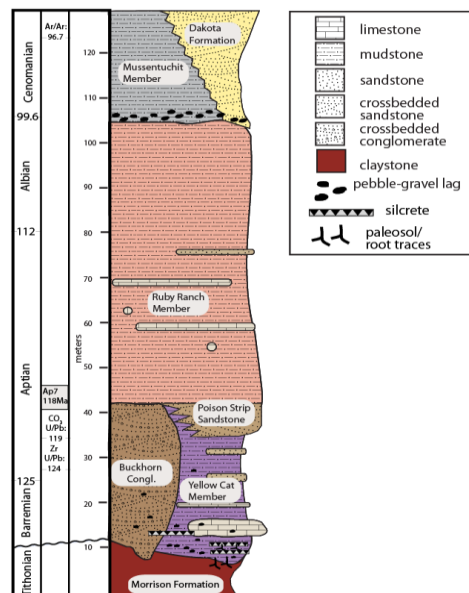
Figure 2. Generalized stratigraphic column of Cedar Mountain Formation with lithologic descriptions and geologic timescale (Modified from Suarez et al., 2014).

The basal members of the CMF are the Buckhorn Conglomerate and Yellow Cat Member. These units unconformably overlie the Jurassic Morrison Formation. The Buckhorn was deposited by a northeast flowing high energy fluvial system draining the Sevier Mountains to the west and Mongollan Highlands to the south (Ludvigson et al., 2010). The Buckhorn type section is located near Buckhorn Reservoir on the northeast side of the San Rafael Swell. It is composed largely of pebble to cobble-sized chert conglomerate and reaches thicknesses of 25m (Kirkland and Madsen, 2007). Chert clasts were sourced and weathered from Paleozoic rocks exposed from early SFTB activity, evident in marine fossils preserved within these gravels (Currie, 2002; DeCelles and Coogan, 2006; Kirkland and Madsen, 2007). The Buckhorn is exposed mostly on the western side of the CMF outcrop belt, mainly in the San Rafael Swell, and is roughly equivalent to the YCM and PSS in some places (Suarez et. al, 2014). Few vertebrate specimens have been recovered from the Buckhorn, but an ankylosaur (armored dinosaur) discovery lends evidence for an early Cretaceous age due to their abundance in the Cretaceous and rarity in the Jurassic (Carpenter and Kirkland, 1998; Kirkland, 2005a).

Where the Buckhorn Conglomerate is absent, the Yellow Cat Member sits atop the Morrison Formation. The YCM was first described as drab mudstones occurring between the Buckhorn Conglomerate or Morrison Formation and the PSS. A calcrete (carbonate-rich paleosol) that overlies and pedogenically alters the Buckhorn conglomerate and/or Morrison Formation was proposed by Aubrey (1998) and Greenhalgh (2006) to represent a large unconformity between the Jurassic and Cretaceous was used as marker for the lower contact of the YCM. But recently, new discoveries of Cretaceous age dinosaurs below this calcrete have suggested that the underlying sediments are some of the earliest Cretaceous deposits, moving the J/K boundary to a

position lower in the section (Kirkland and Madsen, 2007). This calcrete layer has been used to divide the YCM into upper and lower units (Suarez et al., 2014).

The lower Yellow Cat Member consists of drab grayish green to red pebbly siltstones and mudstones containing abundant silicified roots, tree stumps, iron-oxide nodules, and silcretes, which have been interpreted as mature soil horizons (Kirkland and Madsen, 2007). Based on U/Pb zircon dates from an upper Morrison Formation bentonite (Kowallis et al., 2007) and a detrital-zircon date (Britt et al., 2007) from the base of the upper Yellow Cat, the deposition of the lower YCM is constrained to between ~149 to ~124 Ma, but likely has a maximum age of ~136 Ma based on a newly acquired detrital-zircon date from the base of the lower YCM. The lower YCM preserves semi-aquatic taxa such as crocodilians, and terrestrial dinosaurs: basal macronaran sauropods, ankylosaurs, iguanodontids, allosaurids, and small theropods.

The upper Yellow Cat Member consists of poorly sorted pebbly siltstones, lacustrine limestones inter-bedded with red and green mudstones, abundant pedogenic carbonate, spring carbonate, and palustrine carbonate with inter-bedded small-channel sandstone bodies (Suarez et al., 2014). Relative abundance of pedogenic carbonate compared to the lower YCM suggests more arid conditions during upper YCM deposition (Suarez et al., 2014). A U/Pb date of 119 ± 2.6 Ma from pedogenic carbonate from the base of the Poison Strip Sandstone (Ludvigson et al., 2010), constrains the depositional age of the upper YCM from ~124 to ~119 Ma. Vertebrate fauna preserved in the upper YCM include turtles, crocodilians, hybodont sharks, lungfish, semionotid fish, and dinosaurs. Dinosaurs present in the upper YCM include *Utahraptor ostrommaysorum*, the largest known member of the family Dromaeosauridae, polacanthid ankylosaurs, and macronaran sauropods, likely belonging to the family Brachiosauridae.

The Poison Strip sandstone overlies the YCM and is comprised of well cemented medium to coarse cross-bedded to planar-bedded sandstones of fluvial to lake-beach facies. The PSS reaches thicknesses up to 15 m in some places but typically is 4-5 m thick. Young (1960) referred to these resistant, cliff-forming sandstones as the middle Cedar Mountain Sandstone and made the observation that this unit was the most continuous marker bed in the CMF (Kirkland and Madsen, 2007). A basal age of 119 ± 2.6 Ma was obtained by Ludvigson et al. (2010a) for the PSS. Trace fossils (including some of the oldest bird tracks in North America), petrified logs and cycads are common in these sandstones (Dayvault and Hatch, 2005; Kirkland and Madsen, 2007). Dinosaurs are less commonly preserved but overall resemble the upper Yellow Cat fauna (Kirkland and Madsen, 2007).

The Ruby Ranch Member lies atop the Poison Strip sandstone and is characterized by massive reddish and gray mudstones with large carbonate nodules deposited in xeric conditions and contains dolomitized lake deposits and paleosols (Kirkland and Madsen, 2007; Montgomery 2014). The Ruby Ranch Member is prolific, existing everywhere the CMF is recognized and ranges in thickness from 9 m to 90 m (Kirkland and Madsen, 2007; and Garrison et al., 2007). Sediments resemble the Yellow Cat Member but contain many more carbonate nodules representing paleosols and ephemeral ponds formed under semi-arid conditions (Kirkland and Madsen, 2007). Ludvigson et al. (2010) conducted a C-isotope chemostratigraphic study using pedogenic carbonate of the RRM and identified several distinct CIEs such as feature Ap7, described by Herrle et al. (2004), at the base of the member and feature Al1 in the upper RRM. This constrains depositional age of the RRM from the early-mid Aptian (~118 Ma) to the end of the Albian (~100 Ma).

Dinosaur fauna present in this member are distinctly different from older CMF members (Kirkland and Madsen, 2007). Armored ankylosaurs, large primitive ornithopods, and sauropods represented by slender toothed brachiosaurs, form the herbivorous taxa preserved within the Ruby Ranch Member (Kirkland and Madsen, 2007). Theropods include small dromaeosaurids similar to *Deinonychus*, a large undescribed carnosaurid, and the very large, high-spined *Acrocanthosaurus* (Kirkland and Madsen, 2007). Crocodilians and turtles are also present (Kirkland and Madsen, 2007).

The Mussentuchit Member is the youngest member of the CMF and is comprised of gray smectitic mudstones, lignitic mudstones, siltstones, shales and occasional fine-grained sandstones (Suarez et al., 2014). The MM mainly outcrops on the western limb of the San Rafael Swell and sits unconformably atop the RRM, with the contact defined by a zone of chert and quartzite pebbles (Kirkland and Madsen, 2007). Carbonate nodules are less common than in the RRM and suggest a wetter climate as the MM was deposited proximal to the incursion of the Western Interior Seaway (WIS) into eastern Utah and western Colorado (Ludvigson et al., 2010). Volcanic ash layers have dated the Mussentuchit as early Cenomian with an age of 98.37 ± 0.07 Ma (Cifelli et al., 1999).

More than 80 species of small vertebrates have been discovered in the MM, by wet sieving techniques and include fish, frogs, salamanders, turtles, lizards, crocodilians, birds, mammals, and the oldest North American snake (Kirkland and Madsen, 2007). The MM also contains the only known assemblage of fossilized pollen within the CMF described by Tschudy et al., (1984). Dinosaur remains are also common, found mainly as teeth (Kirkland and Madsen, 2007). Herbivorous taxa include ankylosaurids, nodosaurids, ornithopods, pachycephalosaurs, primitive horned dinosaurs, and slender toothed brachiosaurs (Kirkland and Madsen, 2007). Carnivorous

dinosaurs are diverse and abundant and include North America's earliest known tyrannosaurids, coelurosaurs, troodontids, and dromaeosaurine and velociraptorine dromaeosaurids (Kirkland and Madsen, 2007).

B. Tectonics and Climate

The CMF was deposited during the Early Cretaceous in the foredeep, forebulge, and backbulge areas of the Sevier Orogeny foreland basin or the Western Interior Basin (WIB). Initial thrust events began in the Late Jurassic as volcanic arcs and island terrains, associated with the Farralon plate, began accreting along the western margin of North America, causing crustal shortening in Nevada and western Utah (Fig. 3), ultimately leading to the formation of the Sevier Fold and Thrust Belt (SFTB) (Decelles and Coogan, 2006). Two periods of eastward propagating Sevier thrusting took place during the emplacement of the CMF. The Canyon Range thrust occurred during the Aptian – Early Albian (145-110 Ma) and provided sediments to the Yellow Cat and lower Ruby Ranch Members of the CMF, which were deposited in the distal foredeep and proximal backbulge areas of the foreland basin (DeCelles and Coogan, 2006). The Pavant thrust occurred during the Middle Albian – Cenomanian (110-86 Ma) and provided sediments to upper Ruby Ranch Member and the Mussentuchit Member (DeCelles and Coogan, 2006). The upper RRM was deposited in the distal foredeep to forebulge, while the MM was deposited in the foredeep of the Pavant thrust. The Canyon Range thrust is estimated to have increased the regional elevation by ~1.6 km and by the end of the Pavant thrust elevation had increased by ~2.8 km in western Utah (DeCelles and Coogan, 2006).

By the Late Cretaceous, the SFTB formed a high relief mountain chain similar to the Andes Mountains with a high-elevation, low relief hinterland plateau (Currie, 2002; DeCelles and
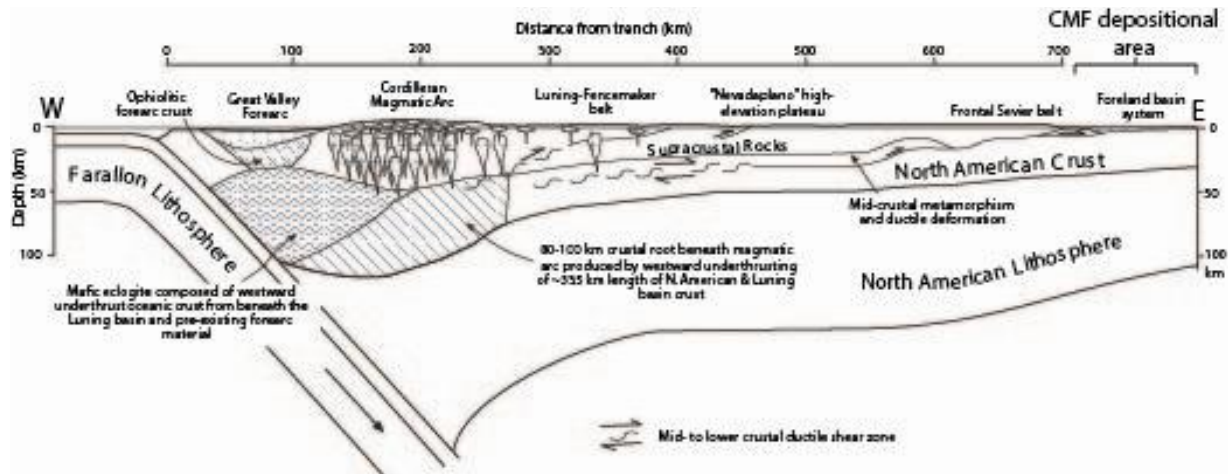
Figure 3. Reconstructed cross-section of the Cordilleran orogenic belt of North America at the latitude of central Utah during the Late Cretaceous, with CMF depositional area depicted. Geology beneath the magmatic arc is after Ducea (2001). Figure modified from DeCelles and Coogan (2006).

Coogan, 2006; Snell et al., 2013), deemed the "Nevadaplano", analogous to the Antiplano of the central Andes Mountains (DeCelles and Coogan, 2006). Through Cretaceous time the WIB continued to subside and as the oceans transgressed, was inundated by the Cretaceous Interior Seaway depositing the overlying Dakota Sandstone and Mancos Shale Formations.

The exposures of the CMF we see today were caused by various tectonic events of western North America. The CMF is deposited within the Paradox basin, named for the underlying Pennsylvanian Paradox Formation which consists of thick sequences of the evaporites salt, anhydrite and gypsum. Salt diapirism occurred from mid-Pennsylvanian through Jurassic time and formed northwest trending bulges, or salt anticlines (Baars and Doelling, 1987). Associated synclines created accommodation space for subsequent deposits including the CMF.

The Laramide Orogeny began around 80 Ma as the formation of large reverse faults, east of the SFTB, created broad areas of uplift forming the Colorado Plateau and numerous basins within. Tertiary volcanics and intrusions also occurred in the area facilitating further uplift and forming the nearby peaks of the La Sal and Henry mountain ranges. In the exposed eroded limbs

and dissected cores of various anticlines, synclines, and monoclines, the CMF and associated formations are exposed.

The Cretaceous climate is characterized by an overall global warming trend reaching a thermal maximum in the Cenomanian-Turonian. A global increase in temperature is thought to have intensified the global hydrologic cycle producing increased rainfall and increased rainout intensity which may explain observances of isotopic depletion of meteoric waters along the eastern margin of the Western Interior basin (White et al., 2001). The global carbon cycle experienced numerous significant fluctuations throughout the Cretaceous indicated by the widespread deposition of organic-rich black shales attributed to global oceanic anoxic events (OAEs). Both global warming and global cooling trends have been observed in marine and near-shore deposits of similar age to the CMF (Suarez et al., 2014). Decreases in $\delta^{18}O$ of marine carbonates and $\delta^{13}C$ of organic matter just before the occurrence of OAE1a (early Aptian, ~120 Ma) suggest an increase of greenhouse gases and a period of global warming (Bellanca et al., 2002). This climatic event, known as the Selli Event, is postulated to have been initiated by the "superplume" submarine eruption of the Ontong Java Plateau, the largest (volumetrically) large igneous province (LIP) in the world covering an area of ~$2.0x10^6$ km^2 and exceeding a volume of over $8.4x10^6$ km^3 (Taylor, 2006). A large influx of CO_2 from this volcanic event would likely have facilitated changes in atmospheric and oceanic conditions globally, increasing the effects of the mid-Cretaceous greenhouse climate leading to increased weathering and erosion and nutrient cycling (Tarduno et al., 1991).

Locally, the rise of the SFTB would have likely affected regional climate and paleohydrology. Eastward moving air masses transported by the paleo-westerlies would have encountered the SFTB (Poulsen et al., 2007) and undergone orographic lifting creating intense rainout on the

windward or western side of the range and likely producing isotopically depleted scant rainfall

on the leeward or eastern side of the range, in which the CMF was deposited (Fig. 4). As
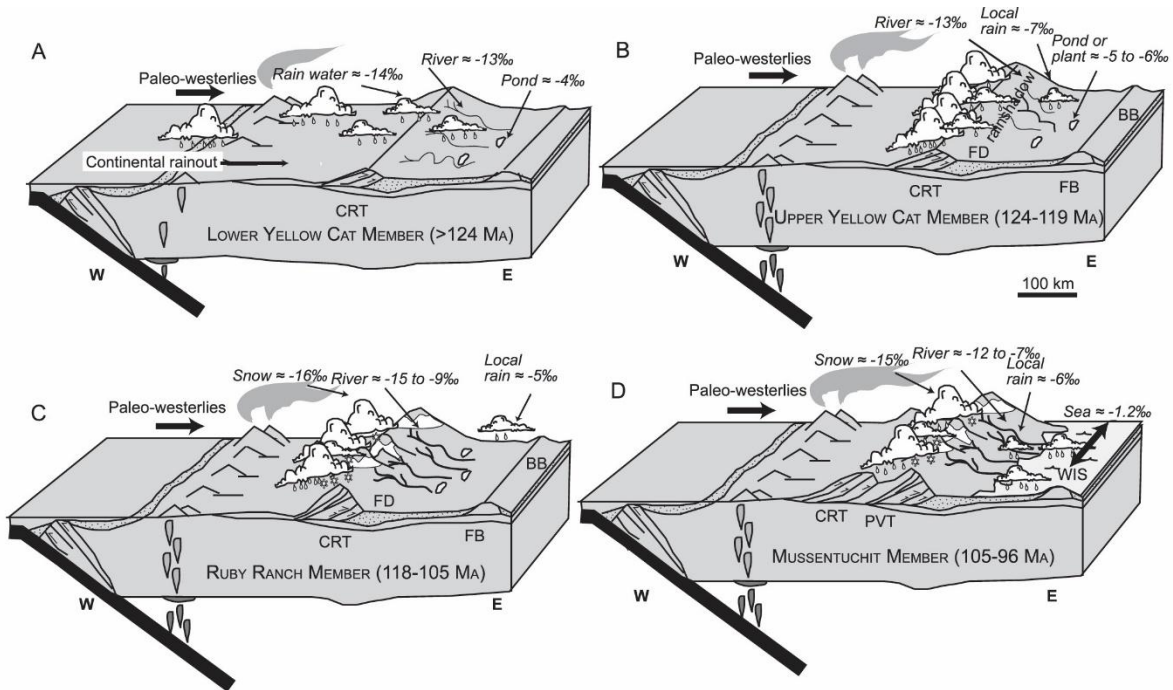
Figure 4. Block diagrams of interpreted paleoclimatic and paleogeographic settings based on oxygen isotopic compositions derived by Suarez et al., (2014). A.) Lower Yellow Cat Member: Canyon Range Thrust initiated SFTB to the west of CMF depocenters, creating isotopic depletion of precipitation due to continental rainout and potential seasonal snowmelt. B.) Upper Yellow Cat Member: Sevier orogeny continues creating significant rainout on western side of range and develops a rain shadow over the leeward side. C.) Ruby Ranch Member: Canyon Range Thrust reaches maximum elevations causing increased rainshadow effect and slight enrichment of meteoric waters. D.) Mussentuchit Member: Pavant Thust is initiated, regional subsidence increases as the incursion of the Western Interior Seaway provides significantly enriched moisture to the region. FD = foredeep; FB = forebulge; BB = backbulge. Figure from Suarez et al., 2014, modified from Elliott et al., 2007.

eastward propagating thrust sheets advanced into Utah the rain shadow affect would have

intensified over the CMF depositional area, but as continual basin subsidence and incursion of

the Western Interior Seaway occurred, orographic rain shadow effects would have been

mitigated by the advance of marine moisture. The present study attempts to further distinguish

global and local terrestrial climatic conditions occurring during CMF time.

C.   Stable Isotopes in Plants and Vertebrate Remains

Stable carbon isotope ratios of plants fluctuate in response to the type of photosynthetic pathways the plants utilize, i.e.: C3, C4, and CAM, and to the environmental conditions (O'Leary, 1998; Farquhar et al., 1989; O'Leary et al., 1992). C3 plants dominated Cretaceous ecosystems since C4 plants were not recognized until the Oligocene and not widely distributed until the Miocene (Cerling, 1999). C3 plants today are characterized by a large isotopic discrimination between organic material and atmospheric CO_2, resulting in carbon isotope ratios ranging from ~-32 to -21‰ (Fig. 5) with an average value of ~-27‰ compared to ~-8‰ for
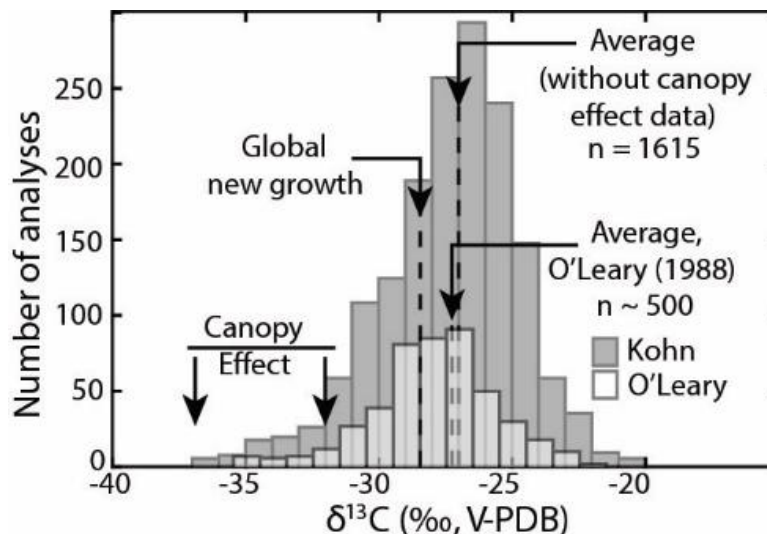
Figure 5. Histogram of $\delta^{13}C$ values of modern C3 plants. Average of -27.0‰ excludes analyses from understory of closed-canopy forests. Estimated global average composition is approximately -28.5‰. Figure from Kohn, 2010.

modern atmospheric CO_2 (Fricke et al., 2008, Kohn, 2010, and others). The range and variability of C3 plant isotopic compositions are due to differing isotopic discrimination for different taxa and to environmental sensitivity within specific taxa (Fricke et al., 2008) Variability of the $\delta^{13}C$ of atmospheric CO_2 through time, from ~-8‰ to ~-5‰, has likely produced a C3 plant isotopic range as much as 3‰ heavier. These fluctuations of atmospheric CO_2 are due to changes in the

amount of volcanic CO_2 emissions, changes in weathering rate, changes in primary productivity in the oceans, and changes in the amount of terrestrial decomposition (Grocke and others).

CO_2 concentrations within a leaf cell are greatly influenced by the opening and closing of leaf stomata, which controls the flux of CO_2 into a plant. When environmental conditions such as temperature, water availability, salinity, nutrient availability, light intensity are such that water needs to be conserved, stomata are more likely to remain closed (O'Leary, 1988; Farquhar et al., 1989; Tieszen, 1991; O'Leary et al., 1992). Relative location of a plant may also influence carbon isotope ratios within the plant. For example, a plant located under a closed forest canopy is exposed to CO_2 that exhibits a lower carbon isotope ratio than the open atmosphere due to plant respiration and decomposition on or near the forest floor (Fricke et al., 2008). Thus, plants living in a closed canopy area have lower carbon isotope ratios than plants of the same species living in open canopy settings (e.g. van der Merwe and Medina, 1991; Cerling et al., 2004). As carbon isotope ratios of atmospheric CO_2 change over time, isotopic values of plant material also change in response and thus, can be used to monitor climatic conditions through time.

Stable oxygen isotope ratios of waters within streams, lakes, and leaves also vary significantly in response to environmental conditions such as temperature and humidity, and the hydrological 'history' of air masses supplying precipitation to surface water reservoirs (Epstein and Mayeda, 1953; Dansgaard, 1964; Rozanski et al., 1993). Present day oxygen isotope ratios of global precipitation range from ~0 to -30‰ (Dansgaard, 1964; Rozanski et al., 1993), and vary due to the preferential incorporation of ^{18}O into condensate as water is precipitated and removed from cooling air masses. As a result, oxygen isotope ratios of precipitation generally decrease as air masses cool while rising over areas of higher elevation, move away from coastal areas, or move from tropical sources toward higher latitudes (Epstein and Mayeda, 1953; Dansgaard, 1964;

Rozanski et al., 1993; Gat, 1996). Thus, oxygen isotope ratios of precipitation for a given area are largely determined by regional temperatures and rainout patterns.

Oxygen isotope ratios of precipitation for an area may differ greatly from surface water reservoirs due to a variety of local hydrological processes (Fricke et al., 2008). As terrestrial vertebrates generally do not consume precipitation directly, it is important to discern these differences between surface water reservoirs to accurately assess oxygen isotope values preserved within vertebrate remains. Ponds and streams in humid areas may retain local precipitation isotope values with little modification, while large lakes and rivers, especially in arid regions, may undergo evaporation that enriches their oxygen isotope ratio due to the preferential incorporation of ^{16}O into the vapor phase. Evaporation of leaf water can also shift oxygen isotope ratios to more ^{18}O enriched values preserved in vertebrates to higher values relative to precipitation (Fricke et al., 2008). Reservoirs draining large areas and that retain water over long periods of time, such as lakes, soil and ground waters, and large rivers, undergo mixing of precipitation that has fallen at different temperatures, varying air mass conditions and different times (Fricke et al., 2008). This results in mixing of isotopic ratios which can make values of surface waters from a given area quite different from local precipitation isotopic values.

The isotopic record preserved in vertebrate teeth and bones are some of the few continental proxies for quantifying environmental or climatic parameters of the Mesozoic (Amiot et al., 2007). Terrestrial vertebrates record the isotopic characteristics of ancient landscapes by ingesting organic material and drinking water from surface water reservoirs and then forming bioapatite $[Ca_5(PO_4, CO_3)_3(OH, CO_3)]$, which is the main component of tooth enamel, dentine, and bone (Fricke et al., 2008). Carbon found in the carbonate component of bioapatite is related to ingested organic material, plants in the case herbivores and meat in the case carnivores. After

an herbivore consumes plant material, the carbon from that plant material is incorporated into a number of different phases including dissolved CO_2 and HCO_3 which are then ultimately incorporated into the animal's bioapatite (Koch et al., 1994; Koch, 1998; Cerling and Harris, 1999; Passey et al., 2005). Isotope fractionation of carbon from these processes results in a carbon isotope ratio of bioapatite carbon that is higher than that of ingested plant material.

Oxygen isotope ratios of vertebrate bioapatite are controlled primarily by ingested water and atmospheric oxygen which contribute to blood/metabolic water (Longinelli, 1984; Luz and Kolodny, 1985; Bryant and Froelich, 1995; Kohn, 1996; Kohn and Cerling, 2002). The isotopic ratio of atmospheric oxygen has remained relatively constant over time and space, ~23‰ (Kohn, 1996), and likely does not influence variations in the oxygen isotope ratios of bioapatite of vertebrates (Fricke et al., 2008). The isotopic offset between ingested surface waters and both phosphate and carbonate portions of bioapatite is controlled by body temperature, which determines the isotopic fractionation between bioapatite and body water, and fractionations that occur during the formation of body water from ingested water (Fricke et al., 2008). Animals with known and constant body temperatures (i.e. homeothermic mammals and birds) can be used with consideration of these fractionations using physiological models that can account for fluxes of oxygen in and out of the body and the oxygen isotope fractionations associated with each metabolic process (Bryant and Froelich, 1995; Kohn, 1996).

Stable isotope ratios of dinosaur remains have not been used extensively to study environmental conditions of the Mesozoic due in part to the fact that isotopic relations or fractionations between ingested carbon and oxygen and tooth enamel carbon and oxygen have not been precisely determined (Fricke et al., 2008). More recently, studies including Fricke et al., (2008) and Tutken (2010) have generated estimated offsets of bioapatite carbonate, for certain

dinosaur taxa, specifically hadrosaurs and sauropods, and bulk organic matter isotope ratios of carbon by comparing isotope ratios of local dinosaur populations to co-existing bulk organic matter and observing a similar offset in multiple populations from different sites of the same representative dinosaur taxa. Specifically, Fricke et al., (2008) observed ~18‰ offset between δ^{13}C of hadrosaur dinosaur remains and bulk sedimentary organic matter and Tutken (2010) observed a ~16‰ offset between δ^{13}C of sauropod dinosaur remains and bulk sedimentary organic matter. These observed offsets were used in this study to estimate δ^{13}C of herbivore diet for the Yellow Cat, Ruby Ranch and Mussentuchit Members, of which sauropod and hadrosaur specimens were sampled.

D.   The Carbon-Cycle and Stable Isotope Chemostratigraphy

The potential for dating and correlating rocks using δ^{13}C trends and excursions is based on the fact that their ^{13}C/^{12}C ratios have varied over time, mostly due to the partitioning of carbon between organic carbon and carbonate carbon reservoirs in the lithosphere (e.g., Shackleton and Hall, 1984; Berner, 1990; Kump and Arthur, 1999; Falkowski, 2003; Sundquist and Visser, 2004 Saltzman and Thomas, 2012). The lithosphere is the largest carbon reservoir and can be divided into 3 separate reservoirs, sedimentary carbonate, sedimentary organic carbon, and the mantle. The ocean-atmosphere system plays a smaller but necessary and important role in global carbon cycling (Fig. 6).

Precipitation of carbonates involves little carbon isotope fractionation relative to dissolved inorganic carbon (DIC), and the δ^{13}C of carbonate is relatively unaffected by temperature changes (~0.035‰/°C; Lynch-Stieglitz, 2003). This results in the δ^{13}C or inorganically and biologically precipitated carbonate in the oceans being very close to that of the DIC in the oceans (Maslin and Swann, 2005). The oceanic DIC is the largest carbon reservoir in the recent ocean-
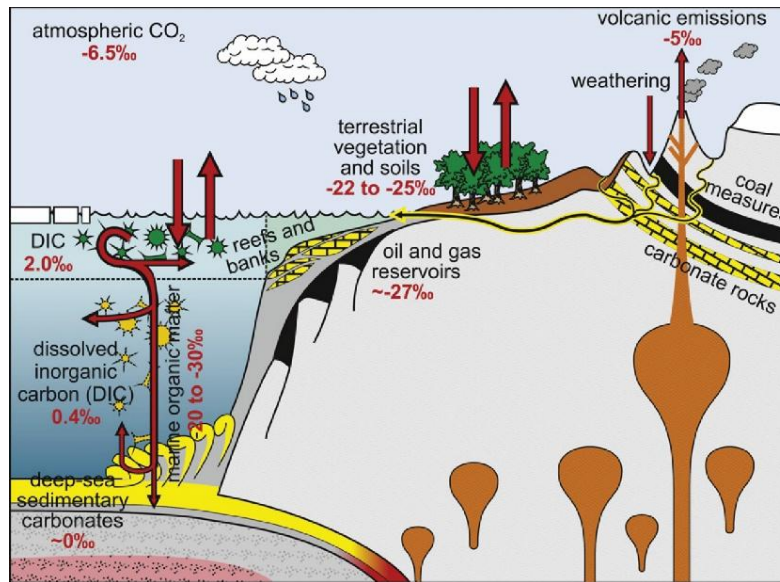
Figure 6. Global carbon cycle diagram showing carbon reservoirs and carbon isotopic compositions vs. VPDB. Volcanic emissions are representative of mantle $\delta^{13}C$ of -5‰. Figure from Saltzman and Thomas (2012) after Dunkley-Jones et al., (2010).

atmosphere system (Saltzman and Thomas, 2012) and is 50-60 times as large as the pre-industrial atmospheric reservoir (Ravizza and Zachos, 2003; Sundquist and Visser, 2004; Sarmiento and Gruber, 2006; Houghton, 2007, Saltzman and Thomas, 2012). Greater than 90% of the carbon in the deep ocean is present as bicarbonate (HCO_3^-). Carbon in the atmosphere is present as carbon dioxide (CO_2). Lithospheric carbon is contained in both organic matter and carbonate rock such as limestones and dolomites. Carbon cycling between the ocean and the atmosphere occurs on time scales of <1000 years, while exchanges between the lithosphere and ocean-atmospheric system is on longer time scales between 100,000-1,000,000 years (Berner, 1990; Saltzman and Thomas, 2012).

The carbon isotopic composition of CO_2 in the atmosphere was about -6.4‰ prior to anthropogenic fossil fuel combustion, and currently is -7.9‰ due to the influx of isotopically light fossil fuels (Francey et al., 1999; Saltzman and Thomas, 2012). The photosynthetic fixation of carbon using atmospheric CO_2 involves a large negative fractionation, so that all organic

carbon compounds are strongly depleted in ^{13}C relative to atmospheric CO_2 (Maslin and Thomas, 2003; Saltzman and Thomas, 2012). Thus, this results in land plants that use the C3 photosynthetic pathway, have δ^{13}C values ranging from ~-32‰ to ~-21‰, with a mean value of ~-26‰.

The δ^{13}C of whole-ocean DIC has not been constant over geologic time. Variations in $\delta^{13}C_{DIC}$ in the oceans over time scales of tens of thousands of years or less can be understood in terms of carbon redistribution between Earth's surface reservoirs, the atmosphere, oceans, biosphere and superficial sediments (Sundquist and Visser, 2004; Saltzman and Thomas, 2012). Changes in size and rate of the exchange fluxes between Earth's surface carbon reservoirs and the lithosphere result in variations in $\delta^{13}C_{DIC}$ over time scales of hundreds of thousands to millions of years (Berner, 1990; Kump and Arthur, 1999; Sundquist and Visser, 2004; Maslin and Swann, 2005, Saltzman and Thomas, 2012). This mostly relates to storage in the lithosphere of varying amounts of carbon as organic carbon relative to the amount stored in carbonates (Saltzman and Thomas, 2012). The lithospheric organic carbon reservoir includes coal, oil and gas, but is mostly comprised of dispersed organic matter (Saltzman and Thomas, 2012). Presently, the out-flux of carbon from the oceans into calcium carbonate is about 4 times as large as the out-flux of carbon into organic matter (Shackleton and Hall, 1984; Shackleton, 1987, Saltzman and Thomas, 2012). If relatively more/less carbon is removed from the oceans in organic matter (relative to carbonate), the $\delta^{13}C_{DIC}$ in the whole ocean increases/decreases (Shackelton, 1987; Berner, 1990; Kump and Arthur, 1999; Hayes et al., 1999; Derry et al., 1992; Des Marais et al., 1992; Ravizza and Zachos, 2003; Sundquist and Visser, 2004; Maslin and Swann, 2005; Saltzman and Thomas, 2012). When there is net oxidation of organic matter globally, the $\delta^{13}C_{DIC}$ in the whole ocean

decreases; when there is net deposition of organic matter globally, the $\delta^{13}C_{DIC}$ in the whole ocean increases (Saltzman and Thomas, 2012).

The $\delta^{13}C_{DIC}$ in the oceans is not only linked to the $\delta^{13}C$ of atmospheric CO_2 through exchange between the atmosphere and surface ocean, but also through circulation between surface and deep waters in the oceans: the "atmosphere is the slave of the ocean" because of its much smaller size (Sundquist and Visser, 2004; Maslin and Swann, 2005, Saltzman and Thomas, 2012). A change in the carbon isotope composition of the large oceanic DIC reservoir is thus reflected in the isotopic composition of other components of the carbon cycle within the time order of circulation of the deep ocean (~1,000 years), such as organic matter in marine and terrestrial sediments (Hayes et al., 1999), plant material (Robinson and Hesselbo, 2004), carbonate nodules in soils (Ekart et al., 1999; Ludvigson et al., 2010), and carbonate in herbivore teeth (Koch et al., 1992).

Carbon Isotope Excursions, (CIEs) may be either positive or negative. Extremely negative CIEs (NCIEs) are likely linked to release of methane hydrates, which have an extremely light C-isotope signature. Methane hydrates are common in young sedimentary packages and can be released by metamorphism, global warming of the oceans and atmosphere, and changes in sea-floor spreading rates (Saltzman and Thomas, 2012). During CMF deposition (~125 Ma), the world's largest Large Igneous Province (LIP) was erupted onto the Earth's surface. The Ontong Java Plateau of the western Pacific Ocean likely formed over a 3 million year period around the Barremian-Aptian boundary (Tarduno, 1991). This greatly increased the abundance of CO_2 in the atmosphere and oceans, likely producing a bloom of photosynthetic organisms and may correspond to PCIEs associated with early Cretaceous OAEs, specifically OAE 1a, or the "Selli Event". Positive CIEs are generally associated with higher rates of burial of organic carbon

19

which is more concentrated in the light carbon isotope (Saltzman and Thomas, 2012), leaving behind a heavier isotopic signature in the world's oceans and atmosphere. CIEs have been associated with episodes of extinction and/or rapid evolutionary turnover resulting from an abrupt rise in temperature, caused by rapid influx of CO_2 into the atmosphere leading to an accelerated hydrological cycle, increased continental weathering, enhanced nutrient discharge to oceans and lakes, intensified upwelling, increased organic productivity, and widespread ocean anoxia and acidification (Saltzman and Thomas, 2012).

III.   Previous Research

A.   Isotope Proxy Studies

Recently, much work had been done to investigate the climatic conditions of the CMF. The $\delta^{18}O$ of phosphate from the same suite of samples being used in this investigation, has been previously analyzed by Suarez et al., (2014) and was used to investigate the regional climatic effects of the formation of the "Nevadaplano" plateau during the Sevier Orogeny. Turtle, crocodile and dinosaur taxa were compared to coeval pedogenic carbonates to interpret changing water sources over time. The isotopic values generated from hydroxlapatite of herbivorous dinosaurs were used to calculate the $\delta^{18}O$ values of dinosaur drinking water, using modifications of $\delta^{18}O_P$ - $\delta^{18}O_{water}$ relationships determined for herbivorous birds by Kohn (1996), and body temperature estimates of dinosaurs from Amiot et al., (2006) and Eagle et al., (2011).

Calcite, turtle, and crocodile isotope compositions imply similar isotopic compositions of water. When the meteoric values calculated from the semi-aquatic taxa of crocodiles and turtles are compared to the calculated drinking water of dinosaurs, the dinosaur ingested waters show a relative depletion by as much as 5-10‰, which Suarez suggests may be due to consumption of

20

water from rivers and streams sourced from higher elevations and snow melt derived from the Sevier Mountains. Calculated values of $\delta^{18}O_w$ and inter-taxon comparisons suggested that sauropods and larger theropods consumed isotopically enriched water relative to small theropods and ornithischians. This is likely due to consumption of more enriched water sources, such as lakes for larger taxa, and more depleted water sources, such as streams and rivers, for smaller taxa. Suarez also concluded that a rainshadow progressively intensified from lower Yellow Cat to Ruby Ranch times (c. 135 to 110 Ma), and snow was likely present at least locally at proximal high elevations primarily from the upper Yellow Cat through Ruby Ranch Member time.

B.   Chemostratigraphic Studies

Various isotope studies of early Cretaceous marine sections (Mengatti et al., 1998; Erba et al., 1999; Bellanca et al., 2002) have been conducted. Relatively little work has been done to construct carbon isotope curves of terrestrial sections or using terrestrially derived organic matter. This is primarily due to the usually low organic carbon content of terrigenous sediments, the lack of age constraining index fossils, and the likely greater frequency of unconformities.

Grocke et al., (1999), constructed an organic carbon-isotope curve of the biostratigraphically well-constrained Aptian shallow-marine siliciclastic succession of the Isle of Wight in southern Britain, derived from the composition of fossil wood fragments. Results indicated that the $\delta^{13}C_{wood}$ was primarily influenced by fluctuations in the isotopic composition of CO_2 in the global ocean-atmosphere system, closely resembling compositions registered in the $\delta^{13}C$ of marine carbonates elsewhere. CIEs were observable in the constructed curve and were correlated with excursions documented in Aptian age Tethyan carbonate platform deposits associated with OAE 1a.

M. Suarez et al., (2013) sampled two Early Cretaceous lacustrine sections of the Xiagou

Formation in the Changma Basin in Gansu Province, China and correlated them using carbon

isotope compositions of bulk organic matter and carbonate based on a two-step increase in

$\delta^{13}C_{org}$ of about 12.5‰. These two sections were correlated with global isotopic variations C3-

C7 observed in marine sections, dating these lacustrine sections as early Aptian, and displaying a

terrestrial manifestation of the CIEs associated with OAE 1a (Fig. 7).
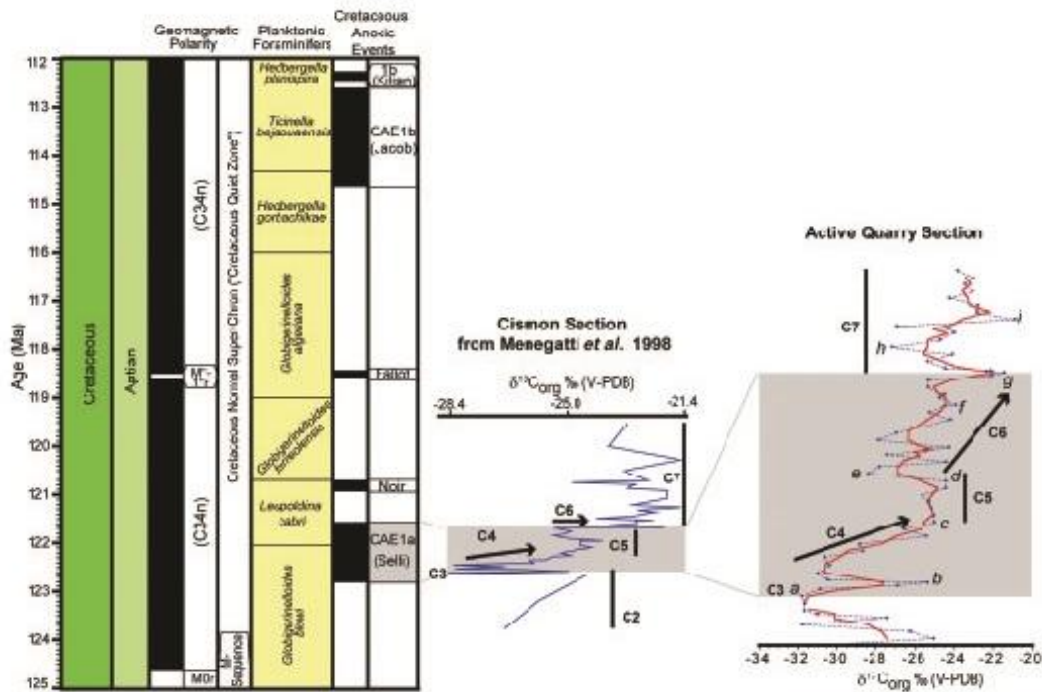
Figure 7. Correlation of Xiagou Formation section, Gansu Province, northwest China from M.B. Suarez et al., (2011) to Cismon section, Italy, from Mengatti et al., (1998). Both chemo-stratigraphic curves show a negative excursion at C3 followed by a two-step positive excursion defined by C4, C5, and C6 which encompass the 'Selli Equivalent' associated with ocean anoxic event 1a (OAE 1a). Figure from M.B. Suarez et al., (2011).

Ludvigson et al. (2010) analyzed $\delta^{13}C$ and $\delta^{18}O$ of pedogenic carbonates from the CMF to

compare with marine record carbon isotope excursions and characterize meteoric-phreatic water

compositions. They found that the terrestrial chemostratigraphy from two measured sections of

the Ruby Ranch member closely correlated with the global marine carbon chemostratigraphic

record and were able to observe CIEs that were previously known from the global record

established from marine deposits from the Vocontian Basin of SE France by Herrle et al. (2004).

Specifically they correlated Aptian to Albian excursions Ap 7 through Al 12 (Fig. 8), providing a

relative depositional age of the Ruby Ranch Member of 118-100 Ma.
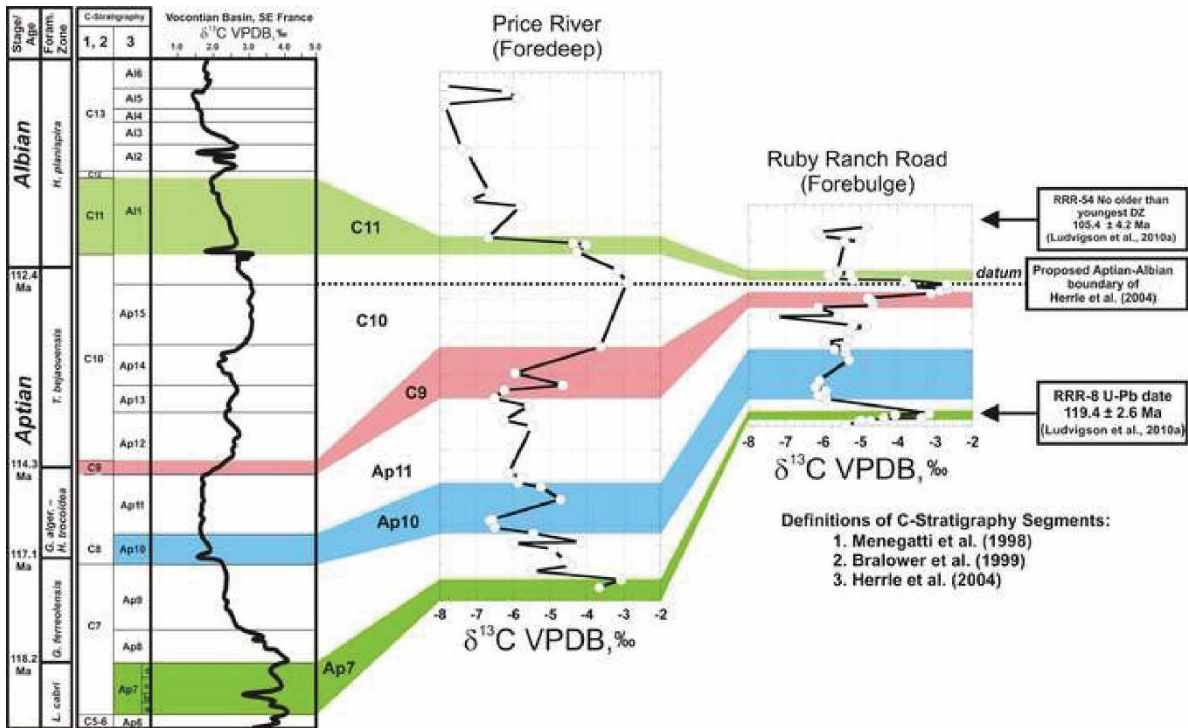
Figure 8. Global correlation of Ruby Ranch member sections of Utah with Vocontian Basin section of southeast France. Figure from Ludvigson et al., (2010a).

IV.   Methods

A.   δ¹³C and δ¹⁸O of Vertebrate Remains

Samples of CMF vertebrate tooth enamel, dentine and bone were provided by several

museum collections: the Oklahoma Museum of Natural History (OMNH), the Utah Museum of

Natural History (UMNH), the College of Eastern Utah Museum (CEUM), the Denver Museum

of Nature and Science (DMNH), and Brigham Young University Museum of Vertebrate

Paleontology (BYUVP). Samples were drilled by hand using a dental drill, producing 1000-2500 µg of powder. Cleaning and analysis of samples was done following Koch et al. (1997). Foreign organic material was removed from the samples by reacting 40 µL of 30% hydrogen peroxide (H_2O_2) per 1 mg of sample. Samples were vortex stirred and allowed to react for 24 hours suspended in an ultrasonic bath that stirred for 15 minutes every hour. After the timed reaction, H_2O_2 was decanted. Samples were then rinsed by adding 1ml of millipore water and centrifuged at 3000 RPM for 10 minutes and then decanted. This was repeated at least 3 times and then samples were dried in an oven.

   Diagenetic carbonate was removed by reacting the samples with 40 µL of 1M calcium acetate-acetic acid buffer solution per 1 mg of sample. Samples were vortex stirred and then suspended in an ultrasonic bath that sonicated for 15 minutes every hour for 12 hours. Samples were centrifuged at 3000 RPM for 10 minutes and the calcium acetate-acetic acid buffer solution was then decanted. Rinsing was performed by adding 1ml of millipore water and centrifuging at 3000 RPM for 10 minutes and then decanted. This was repeated 3 times before drying samples for 24 hours in a vacuum oven. ~1.0 mg of sample (depending on how much sample was left over from the cleaning process) was then weighed using a micro-balance scale, for mass spectrometry analysis and placed in 4.5 ml glass Exetainer vials with membrane lids. Samples were then flushed with helium and reacted with 105% H_3PO_4 (phosphoric acid) overnight to generate CO_2 before being sampled with a Thermo Scientific Finnigan Gas Bench II attached to a Thermo Finnigan isotope ratio mass spectrometer (IRMS) at the University of Arkansas Stable Isotopes Laboratory (UASIL). $\delta^{13}C$ and $\delta^{18}O$ were calculated from the IRMS results. Instrument stability and precision was monitored via analysis of NBS-19, UASIL 22 and UASIL 23 to within 0.15‰.

B. Inorganic $\delta^{13}C$ and $\delta^{18}O$ Chemostratigraphy

0.3 mg, from each non-decarbonated sediment sample, was placed in 4.5 ml glass Exetainer vials with membrane lids. Samples were flushed and pressurized with helium gas. 5-6 drops of 105% H_3PO_4 (phosphoric acid) were injected into each vial and then placed in a heating block at 25°C to react with the sample overnight to generate CO_2 gas which was then sampled with a Thermo Scientific Finnigan Gas Bench II attached to a Thermo Finnigan IRMS at UASIL for $\delta^{13}C$ and $\delta^{18}O$. Instrument stability and precision was monitored via analysis of NBS-19, UASIL 22 and UASIL 23 to within 0.1‰ standard deviation. Sample $\delta^{13}C_{carb}$ and $\delta^{18}O_{carb}$ values were then graphed against stratigraphic position, generating carbon and oxygen isotope chemostratigraphic curves.

C. Bulk Organic $\delta^{13}C$ Chemostratigraphy

Several grams of rock material from each of 66 samples taken at 0.25 m intervals were ground into a powder by use of mortar and pestle. One to two grams of powdered sample were then weighed into 50ml centrifuge tubes and reacted with 30ml of 0.5M hydrochloric acid (HCl) at room temperature to remove inorganic carbonate. The samples were reacted for 12 hours and vortex stirred every 3-4 hours. Other HCl concentrations, temperatures, and reaction times were also used in separate successive de-carbonation reactions of selected samples to observe how results were affected by changes in methodology. These successive de-carbonation reactions used either 3M HCl at 60°C for 2 hours or 3M HCl at room temperature for 12 hours. After the initial timed reaction, pH of the samples was tested to see if neutralization had occurred. Samples were then centrifuged at 3000 RPM for 15 minutes and decanted. Another 10 ml of HCl were then added to each sample to see if any noticeable reaction would occur. If a reaction

did occur, then another 20 ml of HCl were added and allowed to react for at least another hour at the appropriate temperature.

After completing the reaction, samples were again centrifuged at 3000 RPM for 15 minutes and decanted. Samples were then rinsed by adding 40 ml of millipore filtered water, stirred via vortex shaker, centrifuged and decanted. This rinsing was repeated at least 3 times and pH of the solution was measured after each rinse until the pH was that of the rinse millipore water (pH ~ 7). Samples were then dried in an oven for 12-24 hours. After drying, samples were then re-crushed by use of mortar and pestle and placed in vials with appropriate labels.

De-carbonated re-powdered samples were then weighed appropriately, between 3-18 mg based on estimates of total weight percent of organic carbon, using a micro balance scale for mass spectrometry analysis. Samples were wrapped in tin capsules which were then combusted in a Thermo Finnigan NC2500 Elemental Analyzer attached to a Thermo Finnigan Delta Plus IRMS at the UASIL to determine $\delta^{13}C$. Instrument stability and precision was monitored via analysis of UASIL lab standards Black Weeks 036 with an average value = -25.09‰ and σ = 0.676, White River trout with an average value = -26.63‰ and σ = 0.118, and Corn maize with an average value = -11.32‰ and σ = 0.059, to within 0.8‰ of actual values. Sample $\delta^{13}C$ values were then graphed against stratigraphic position to generate a carbon isotope chemostratigraphic curve.

V.   Results

A. $\delta^{13}C$ and $\delta^{18}O$ of Vertebrate Remains

$\delta^{18}O$ of vertebrate apatite carbonate was compared to and graphed vs. $\delta^{18}O$ of PO_4 results

from samples analyzed by Suarez et al. (2014). Results were graphed in comparison to the equilibrium equation:

$$\delta^{18}O_{PO4} = 0.98*(\delta^{18}O_{CO3}) - 8.5 \qquad (1)$$

derived by Iacumin et al., (1996), and were grouped by individual taxa for each depositional member (Fig. 9,10, and 11). Some sample values fall close to the line of best fit equation determined by Iacumin indicating the preservation of primary isotopic values, while other sample values lie away from this line, indicating that diagenetic alteration has likely occurred. Iacumin et al., (1996) suggests that values falling off the equilibrium line represent samples that have undergone diagenetic alteration to either the $\delta^{18}O_{PO4}$ or, more likely, the $\delta^{18}O_{CO3}$.
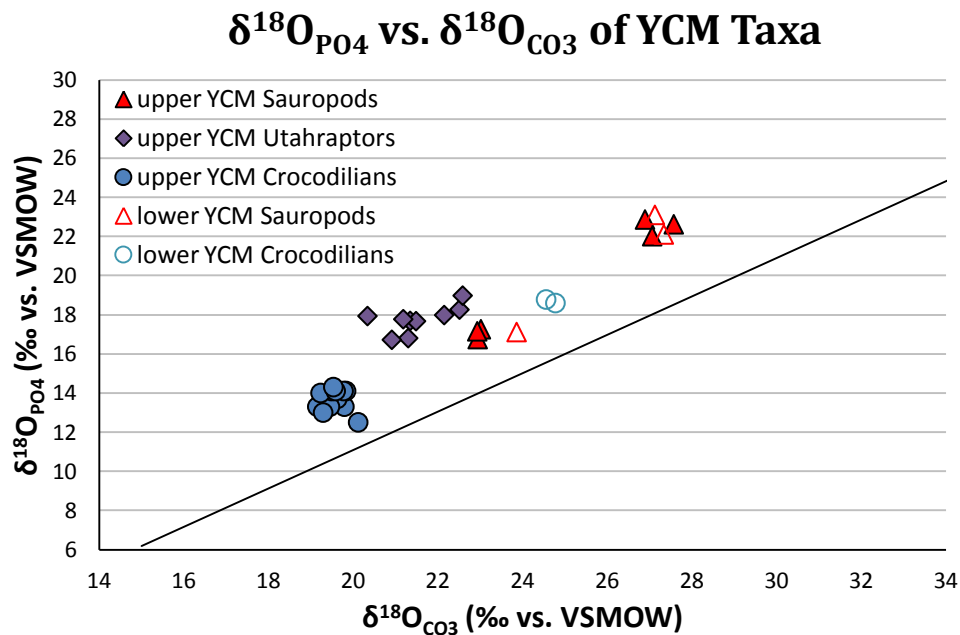
Figure 9. $\delta^{18}O_{PO4}$ vs. $\delta^{18}O_{CO3}$ of Yellow Cat Member vertebrate samples, comparing results to equilibrium trend line of Iacumin et al., 1996, derived from unaltered enamel samples.

All YCM samples fall above the Iacumin et al. line and are all very tightly grouped. These samples all would fall on a trendline with a nearly identical slope as the Iacumin et al. line. Either a slight degree of near identical diagenesis has occurred for all these samples or
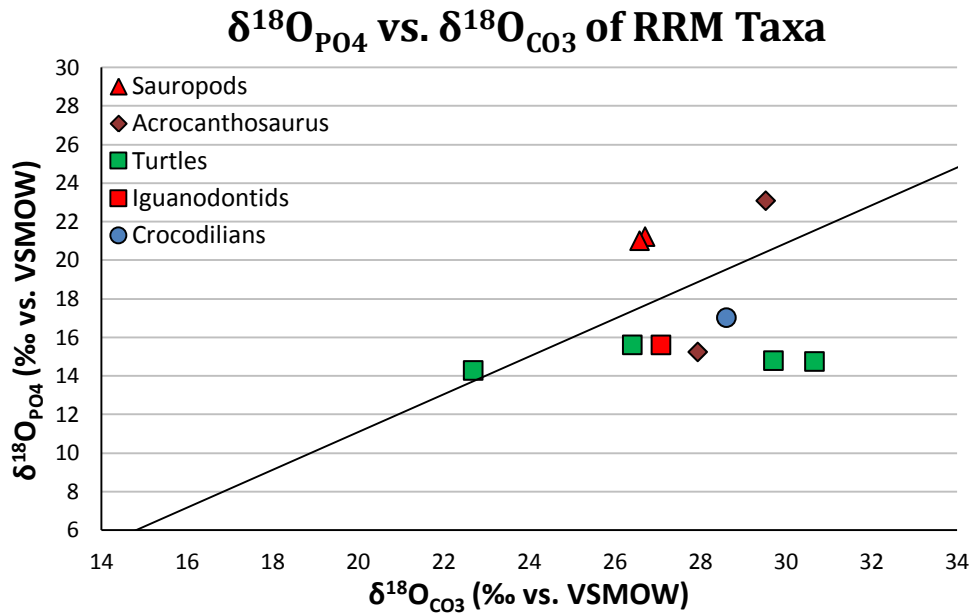
Figure 10. $\delta^{18}O_{PO4}$ vs. $\delta^{18}O_{CO3}$ of Ruby Ranch Member vertebrate samples, comparing results to equilibrium trend line of Iacumin et al., 1996, derived from unaltered enamel samples.
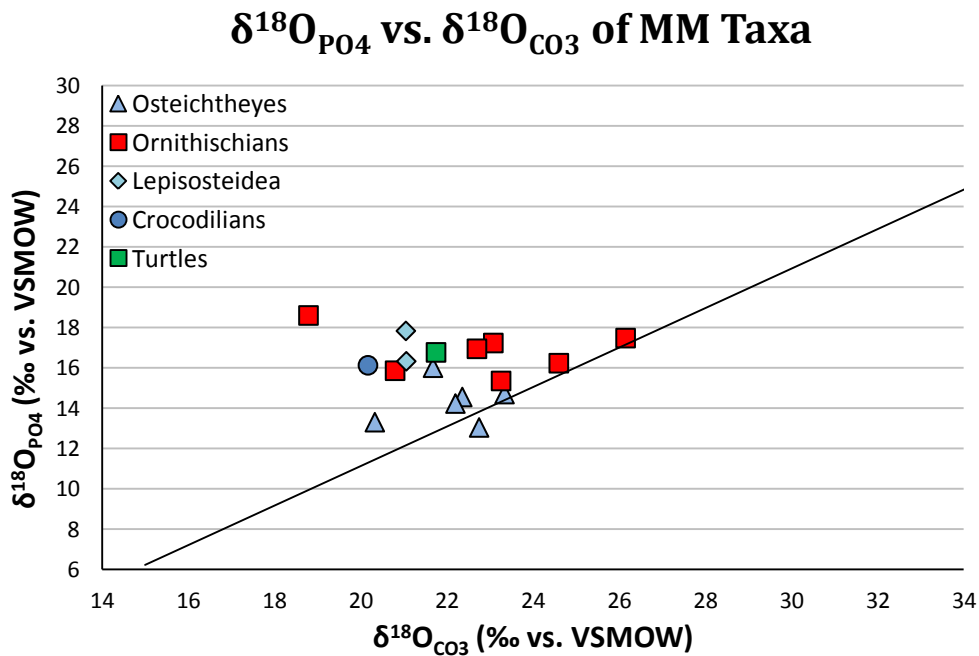
Figure 11. $\delta^{18}O_{PO4}$ vs. $\delta^{18}O_{CO3}$ of Mussentuchit Member vertebrate samples, comparing results to equilibrium trend line of Iacumin et al., 1996, derived from unaltered enamel samples.

a difference in methodology from samples used by Iacumin et al. and the samples used in this study exists. Most RRM samples fall closely on both sides of the Iacumin equilibrium line and indicate preservation of primary isotopic signals. Two turtle samples fall a bit further away from the equilibrium line and have likely been diagentically altered. This is likely since the turtle samples consist of bone which has much more porosity that tooth enamel and is more easily altered after burial by exchange with diagenetic fluids. MM samples fall just above or on the equilibrium line of Iacumin et al., 1996. One outlying ornithischian sample has likely been diagenetically altered.

   The $\delta^{13}C_{CO3}$ of herbivores was used to estimate the $\delta^{13}C$ of herbivore diet using the offsets calculated by Tutken et al., (2010) for sauropods and Fricke et al., (2008) for ornithopods. The estimated $\delta^{13}C$ of herbivore diet was then used in conjunction with the mean annual precipitation equations derived by Kohn (2010) and Diefendorf et al., (2010) to estimate an averaged mean annual precipitation value for each depositional member of the CMF. The following equation, modified from Kohn (2010), was used to calculate MAP:

$$\log_{10}MAP + 300 = (0.17*\Delta) - 0.342 - (0.00219*Abs\ (latitude)) \qquad (2)$$

$$, and\ \ \Delta = (\delta^{13}C_{atmosphere} - \delta^{13}C_{plant}) / [\ 1 + (\delta^{13}C_{plant} / 1000)] \qquad (3)$$

In order to improve the quality-of-fit for the logarithmic regression to the global dataset, Kohn (2010) adds 300 to MAP (see equation 2). This is because regressing the $\delta^{13}C$ vs logMAP data unrealistically approaches negative infinity for $\log_{10}MAP$ and positive infinite for d13C values at lower and lower MAP. Thus, adding 300 to $\log_{10}MAP$ improves R^2 values and eliminates unrealistic predicted $\delta^{13}C$ values at low MAP. This results in a negative MAP for heavier $\delta^{13}C$ values measured in this study. Thus, we eliminated the +300 from the Kohn (2010) equation (see also Kohn, 2010, supplemental data #7). Paleo-latitude for the CMF is estimated at 34°N from

leaf physiognomy and mean annual temperature estimates from Spicer and Corfield (1992) and Wolfe and Upchurch, (1987). An estimate of paleoaltitude which is a factor in the Kohn (2010) equation was not considered because paleoelevation must be greater than ~3 km to greatly affect calculated MAP. $\delta^{13}C_{atmosphere}$ was estimated to be -5.8‰ for the YCM and -6.0 for both the RRM and MM (Ekart et al., 1999). The estimated and averaged MAP value for the lower YCM is 768 mm/yr. The upper YCM had the lowest estimated MAP of all the CMF members at 85 mm/yr. The MAP of the RRM was estimated to be 274 mm/yr., and the MM had the highest estimated MAP, as expected, of 883 mm/yr. (Fig. 12).
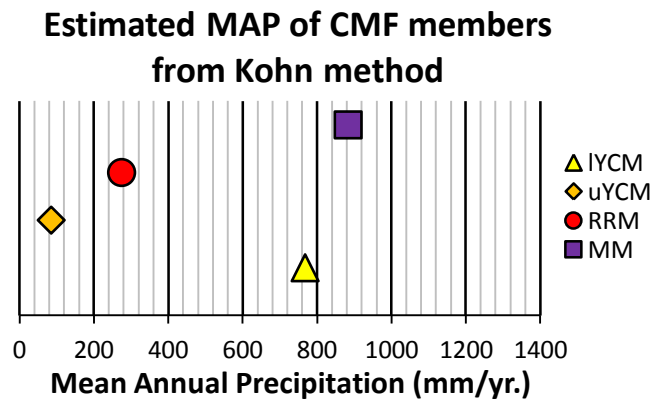
Figure 12. MAP estimates derived from $\delta^{13}C$ of tooth enamel samples using the Kohn (2010) equation.

Diefendorf et al., (2010) used a slightly different equation to derive MAP:

$$logMAP = (0.0802*\Delta) + 1.3726 \qquad (4)$$

with Δ being equal to equation 3. Paleolatitude and estimated $\delta^{13}C$ were the same values used with the Kohn (2010) equation. The resulting MAP estimate for the lower YCM was 849 mm/yr. and the upper YCM was 448 mm/yr. MAP for the RRM was estimated to be 599 mm/yr., and the MM had a MAP value of 910 mm/yr. (Fig. 13). Results differed between the two equations but preserved the same pattern of a decrease of MAP from the lower to upper YCM, a slight increase in MAP relative to the upper YCM for the RRM and a large increase in MAP for the MM.
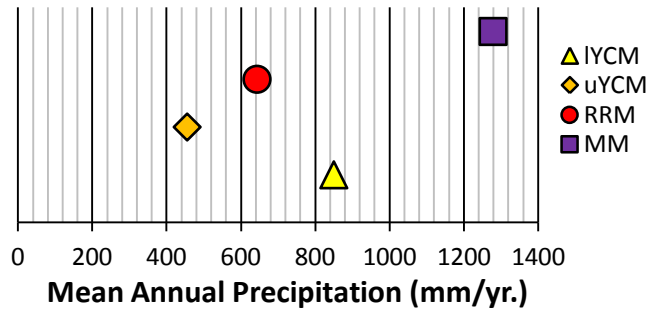
Figure 13. MAP estimates derived from δ¹³C of tooth enamel samples using the Diefendorf et al., (2010) equation.

B. δ¹³ C and δ¹⁸O Chemostratigraphy

A chemostratigraphic curve was constructed from δ^{13}C values of bulk organic carbon derived from paleosol and lacustrine deposits from the upper and lower Yellow Cat Member at a site known as Lake Madsen (LMDS) (Fig. 14). The δ^{13}C of bulk organic material ranged from -22.72 ‰ to -26.76 ‰ with a mean value of -24.49 ‰ relative to VPDB. Values show an overall decrease for the lower half of the YCM and an overall increase for the upper half. Distinct negative trends, possible NCIEs, are observed at 4.5-5 m, 7.5-8.25 m and 10-10.75 m above the J/K contact. A -2‰ spike is observed at the base of the section. Values then increase by >2‰ and oscillate back and forth by ~1‰ from 0.75-4.25m. An increase of 1.5‰ occurs at 4.5m and records the maximum value of the curve at -22.72‰. A decrease of 2.5‰ occurs from 4.5-5.25m. Values slowly increase by ~1‰ from 5.25-7.75m. At 8.25 m the minimum value of -26.76‰ is reached with a negative excursion of ~2.5‰ from 7.75-8.25 m. Values then increase by ~2‰ from 8.25-8.75m. An overall decrease of 1.25‰ occurs between 8.75-10.75 m. From 10.75-14.75 m the curve oscillates back and forth but shows an overall increase of ~2.5‰. From

31
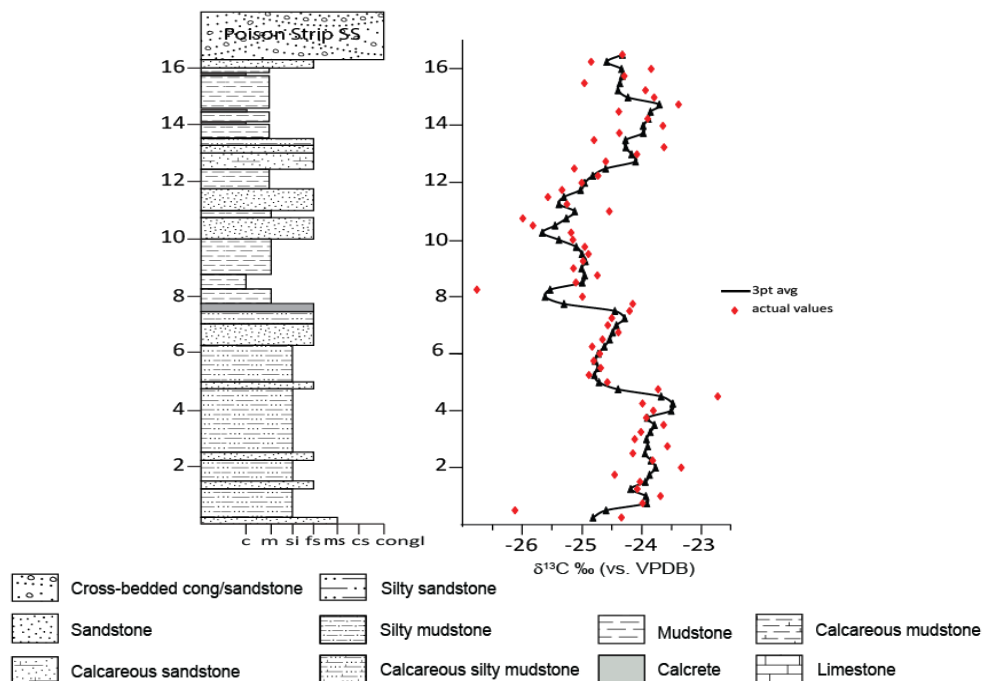
Figure 14. Stratigraphic column with lithologic descriptions of Lake Madsen Discovery Site (LMDS), Yellow Cat Member of the Cedar Mountain Formation, with chemostratigraphic profile of δ^{13}C values obtained from this section.

14.75-16.25 the curve again oscillates back and forth but shows an overall decrease of ~1.25‰.

A three-point running average was created for comparison with other chemostratigraphic curves

of similar age, as that is the practice employed in the comparison of C-isotope curves in an effort

to reduce the effect of outlying values or "noise" on the overall appearance of the curves.

δ^{13}C and δ^{18}O values of inorganic carbonate were also used to construct additional

chemostratigraphic curves (Fig. 15). Values for inorganic carbonate were only obtained for the

upper 8.5 m of the LMDS section due to a lack of bulk carbonate in the lower half of the

sampled section. Starting at 7.75 m, a small negative trend is observed in both curves followed

by a small positive trend from 8-8.75 m. Both curves then display a large negative trend from 9-

9.75 m of almost a 4‰ decrease for carbon and nearly 3‰ decrease for oxygen. Values then

increase for both curves from 9.75-10.25m, with an increase of 4‰ for carbon but only a 1.5‰
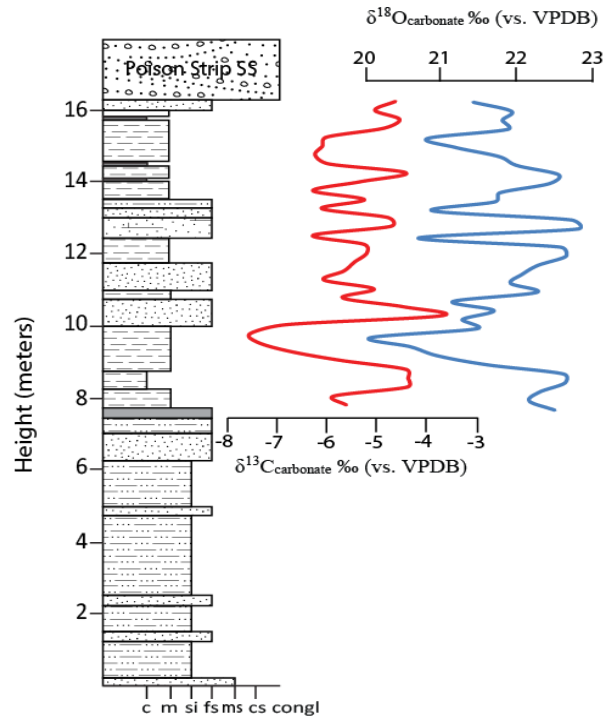
Figure 15. $\delta^{13}C$ and $\delta^{18}O$ chemostratigraphic curves of bulk sedimentary carbonate with lithologic stratigraphic column of LMDS. Note that below the calcrete layer there was not enough carbonate available in samples to derive isotopic values.

increase for oxygen. Subsequently, the carbon values again decrease by 1.5-2‰ from 10.25-10.75 m, while the oxygen values show a small decrease of ~0.5‰ from 10.25-10.5 m followed by a ~1‰ increase from 10.5-11 m, with a small increase, ~0.5‰, for carbon between 10.75-11m. From 11-13.25m both isotope ratios show a strong coupling as they increase or decrease with a range of ~1.5-2‰. Negative spikes are observed in both curves at 11.25, 12.5, and 13.25 m. Positive peaks are observed at 12.25 and 13 m. A negative peak is observed in the carbon isotope curve at 13.5 while the oxygen isotope curve increases. A strong positive peak is observed in both curves at 14 m. Both curves then decrease by ~1.5‰ from 14-15.25 m and increase by ~1‰ from 15.25-15.75 m. From 16-16.25 m carbon values show a small increase, while oxygen values show an equally small decrease.

33
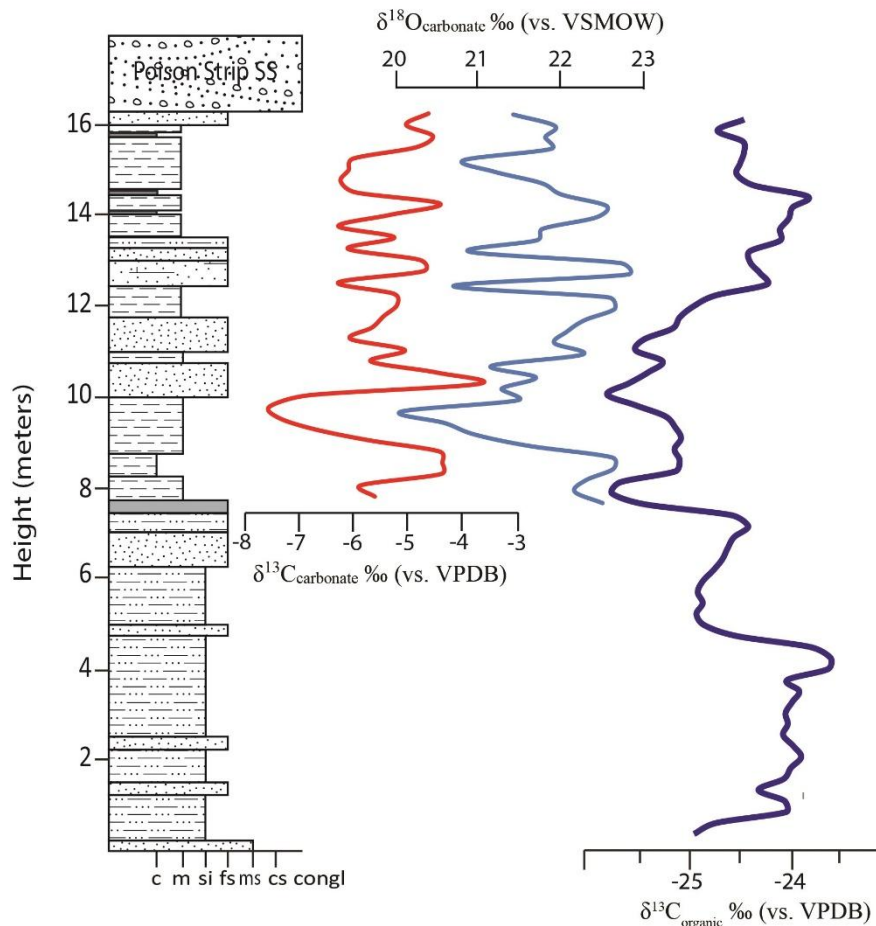
Figure 16. Organic carbon $\delta^{13}C$ chemostratigraphic profile compared alongside chemostratigraphic profiles of $\delta^{18}O$ and $\delta^{13}C$ from carbonate. Overall they show numerous similarities but do have some points of diverging values.

When the inorganic carbonate and organic carbon curves are compared to each other they have an overall similar appearance, suggesting that shifts observed in both curves are controlled by changes in global atmospheric isotope reservoirs and should be comparable to chemo-stratigraphic profiles from other locations from the same time period (Fig. 16).

The isotope curves generated from carbonate show a covariance between the carbon and oxygen values and suggest a freshwater lake system (Fig. 17) (Leng et al., 2006). This isotopic observance coincides with lithological interpretations made for the upper YCM Lake Madsen section.
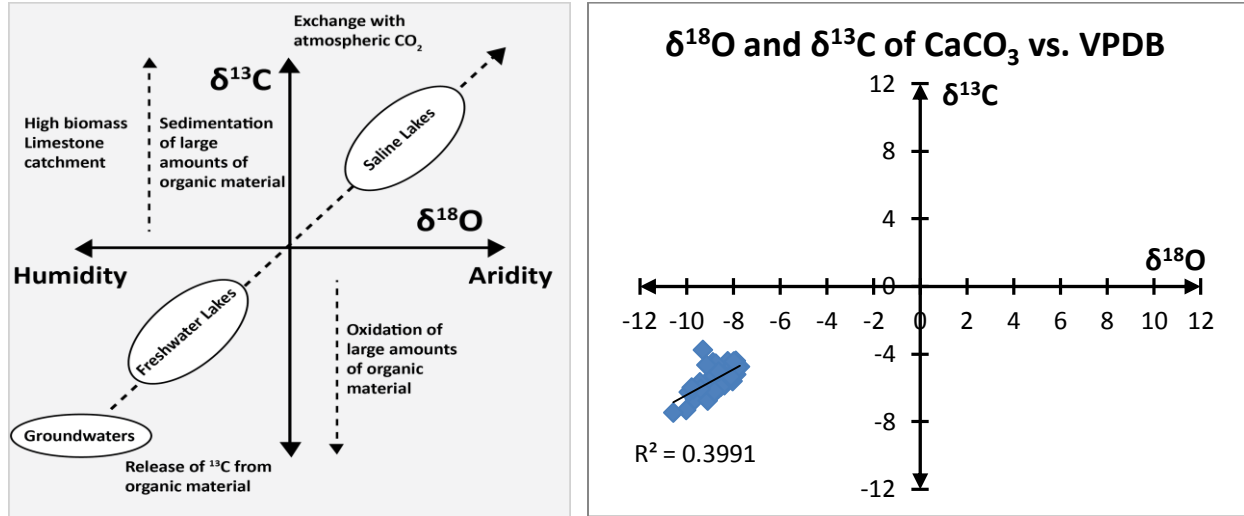
Figure 17. Figure from Leng et al., 2006, showing δ^{13}C vs. δ^{18}O of lakewaters. Plot of δ^{13}C vs. δ^{18}O of inorganic $CaCO_3$ from upper YCM Lake Madsen site. This plot suggests a freshwater lake system with some possible groundwater interaction.

VI.   Interpretations/Discussion/Implications

A. δ^{13}C and δ^{18}O of Vertebrate Remains

$\delta^{18}O_{PO4}$ and $\delta^{18}O_{CO3}$ comparisons show that most samples preserve primary isotopic

compositions when plotted against the equilibrium line of Iacumin et al., 1996. However, some

samples fall off this line, indicating that some diagenetic alteration has occurred, changing the

isotopic composition of the original material. It should be noted however, that the data used to

generate the equation by Iacumin et al., (1996) were generated using the bismuth phosphate

method and analysis via fluorination of bismuth phosphate. This method is known to vary from

the modern method of precipitation of silver phosphate and analysis via combustion in a TCEA

by -1‰ (Chenery et al., 2010). Thus, the y-intercept of the Iacumin et al. (1996) equation should

be increased by 1‰. When we do this, most values fall either on or much closer to the

equilibrium line, except for RRM samples which now mostly fall below the equilibrium line. (Fig. 18, 19, and 20).

The covariance of the data and proximity to the d18Oc-d18Op line of Iacumin et al. (1996) suggests that the $\delta^{18}O_{CO3}$ and $\delta^{13}C_{CO3}$ retain authigenic biologic signals. Additionally, Wang and Cerling (1994) created a mass balance model to recreate burial diagenesis to bone and tooth enamel to determine if carbon and oxygen are altered at the same instance and rate. Based on their data, they suggest that the oxygen component of the carbonate molecule is more likely to be altered than the carbon component. Thus, our data and previous research suggests that the $\delta^{13}C_{CO3}$ represents primary or near-primary isotopic compositions.
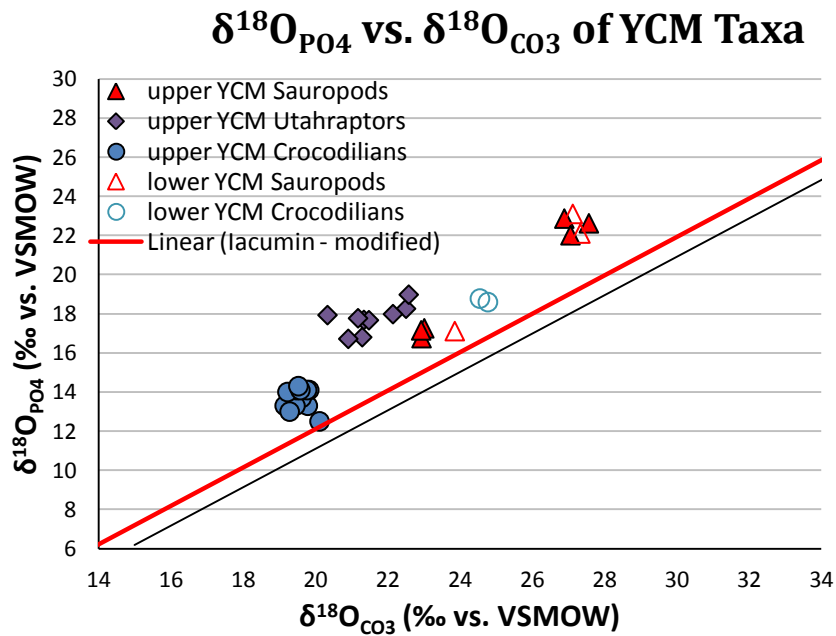
Figure 18. $\delta^{18}O_{PO4}$ vs. $\delta^{18}O_{CO3}$ of Yellow Cat Member vertebrate samples, comparing results to modified equilibrium trend line (in red) of Iacumin et al., 1996.

36

δ¹⁸O_PO4 vs. δ¹⁸O_CO3 of RRM Taxa
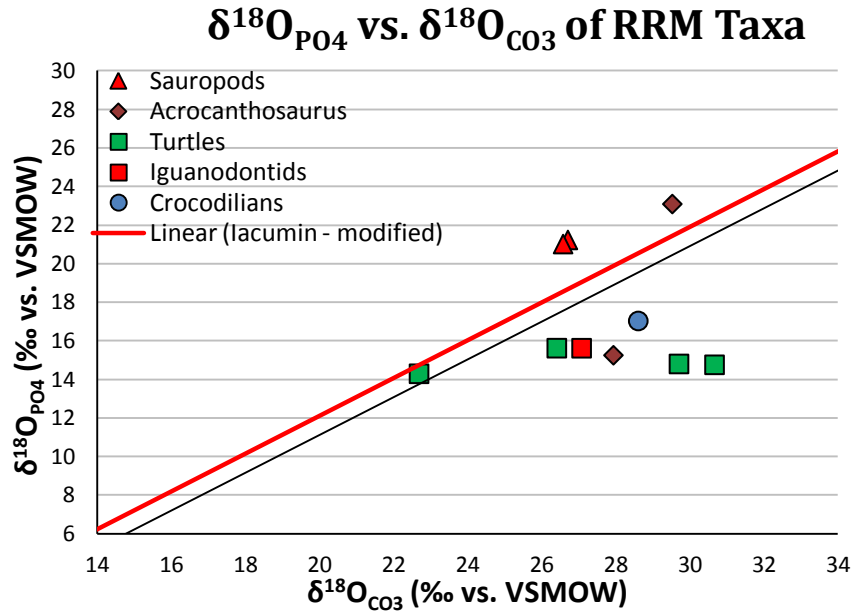
Figure 19. $\delta^{18}O_{PO4}$ vs. $\delta^{18}O_{CO3}$ of Ruby Ranch Member vertebrate samples, comparing results to modified equilibrium trend line (in red) of Iacumin et al., 1996.

δ¹⁸O_PO4 vs. δ¹⁸O_CO3 of MM Taxa
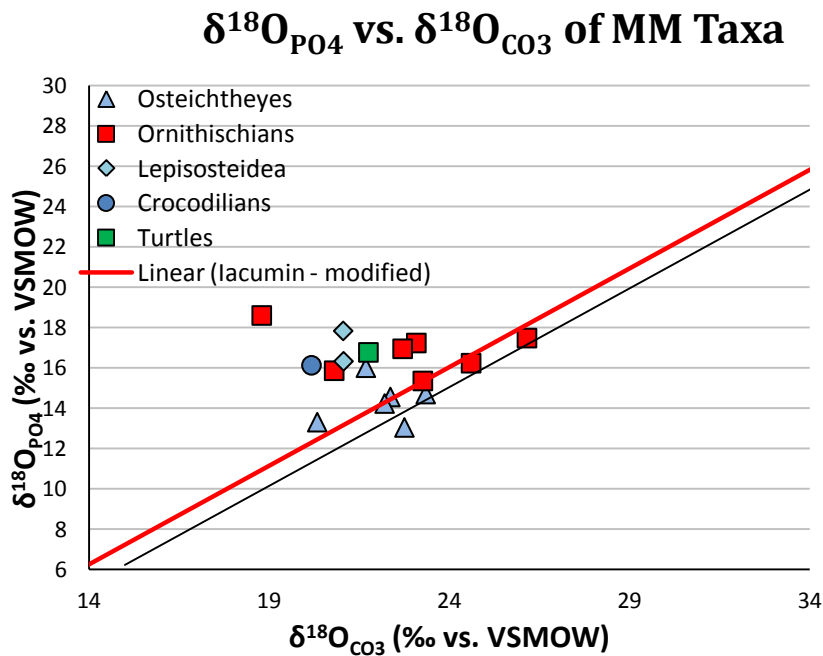
Figure 20. $\delta^{18}O_{PO4}$ vs. $\delta^{18}O_{CO3}$ of MussentuchitMember vertebrate samples, comparing results to modified equilibrium trend line (in red) of Iacumin et al., 1996.

δ^{13}C values obtained from enamel of vertebrate specimens of the CMF allowed for estimation of isotopic compositions of diet or δ^{13}C$_{plants}$ which was then used in the computation of MAP values of depositional members. MAP of the CMF changed through time as the advance of the Sevier Fold and Thrust belt from the west and the Western Interior Seaway from the east encroached upon the depositional area of the CMF. Results show a marked decrease in MAP in the upper YCM, suggesting a more arid environment. This sharp decrease likely arises from activity of the Canyon Range thrust sheet within the SFTB.

From the upper YCM to the Ruby Ranch, MAP values show a slight increase, which is a bit puzzling. The presence of much more sedimentary carbonate than the upper YCM and dolimitized lake deposits found in the RRM suggest a more arid environment. More proximal thrusting associated with the Pavant Thrust during this time would also predict a more arid environment and a greater rain shadow effect than was present in the upper YCM. This may suggest that δ^{13}C values from vertebrate remains of the RRM used to generate the MAP estimate may be diagenetically altered or that indeed the rain shadow effect was somehow mitigated by increased regional subsidence or some other factor.

From the Ruby Ranch member to the Mussentuchit Member, MAP shows a large increase and the value is typical of a humid environment, showing that any rain shadow influence had been erased by coastal moisture inundation. The trends in the MAP calculations follow the interpretation of Suarez et al., (2014), which suggested by the shifts in δ^{18}O$_{PO4}$ that a rain shadow initiated by the upper YCM-time, persisted through the RRM, and ceased by MM-time due to advancing moist air masses from the encroaching Western Interior Seaway.

B. δ^{13} C and δ^{18}O Chemostratigraphy

The Lake Madsen chemostratigraphic curves were compared to various early Cretaceous marine sections looking for similar patterns of CIEs. Correlations were made with the Tethyan carbonate platform Cismon Valley section of the Italian Alps (Erba et al., 1999) on the basis of comparing magnitudes of excursions and patterns of positive and negative trends away from the mean value. An upper age constraint of 119 Ma was used for the Lake Madsen section based on an absolute age date obtained by Ludvigson et al., 2010, which sampled a carbonate layer not present in the Lake Madsen section located just below the Poison Strip Sandstone Member. Correlation indicates a lower Aptian age for the upper YCM and an upper Barremian age for the lower YCM. This is based on the identification of the B5-B8 excursions of the Barremian from 1.0 m to 8.0 m and the A1-C5 excursions of the Aptian from 9.0 m to 16.25 m (Fig. 21). The
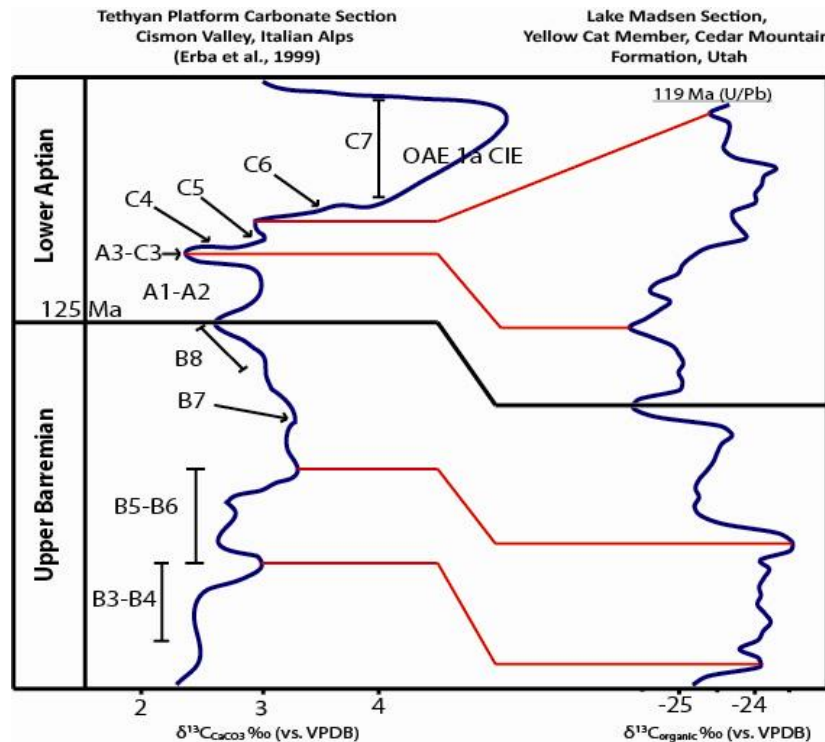
Figure 21. Global chemostratigraphic correlation of the Lake Madsen discovery site section of Utah, and the Cismon Valley Tetyhan platform carbonate section of the Italian Alps. Lake Madsen section is hung from the 119 Ma U/Pb age date obtained by Ludvigson et al. (2010a). Correlation is based on patterns of peak values and amount of offset from mean value.

39

reason that the C4-C5 section is not correlated to the C6-C7 PCIEs is that the magnitude of the excursion is not great enough. Instead, it is assumed that depositional rate increased for the upper 6.25 m as the depositional regime transitioned from a fluvial to lacustrine system. The large C6-C7 PCIE is believed to occur in the Poison Strip Sandstone and has been documented at the base of curves derived by Ludvigson et al., 2010a (see Fig. 8).

C. Problems Encountered

Results for the upper YCM $\delta^{13}C$ of bulk organics were poorly replicated. Values from initial and subsequent IRMS runs varied significantly (Fig. 22). This may have been caused by a number of factors. One possible explanation is that samples were not completely homogenized by crushing with a mortar and pestle, preserving inorganic carbonate when reacted with HCl. This may be the most likely explanation as the largest discrepancies were observed in samples that contained the largest weight percent of inorganic carbonate. Another explanation may be that the porcelain mortar and pestle may have contributed material skewing the isotopic ratios of resulting values. If this is the case, this can be avoided in future studies by using an agate mortar and pestle.

Changes of HCl molarity and temperature were made between the initial and subsequent runs in order to observe possible differences in results. The initial runs were cleaned of inorganic carbonate utilizing 0.5M HCl at room temperature while subsequent runs of the upper 4.75 meters of the section used 3.0M HCl heated to 60°C. This was done to determine if other carbonate minerals could be present in the sediment samples that possess temperature dependent dissolution reactions with HCl, such as dolomite or siderite that may not have been removed with "cold" and weaker HCl. Initial sample weights were compared to sample weights after the
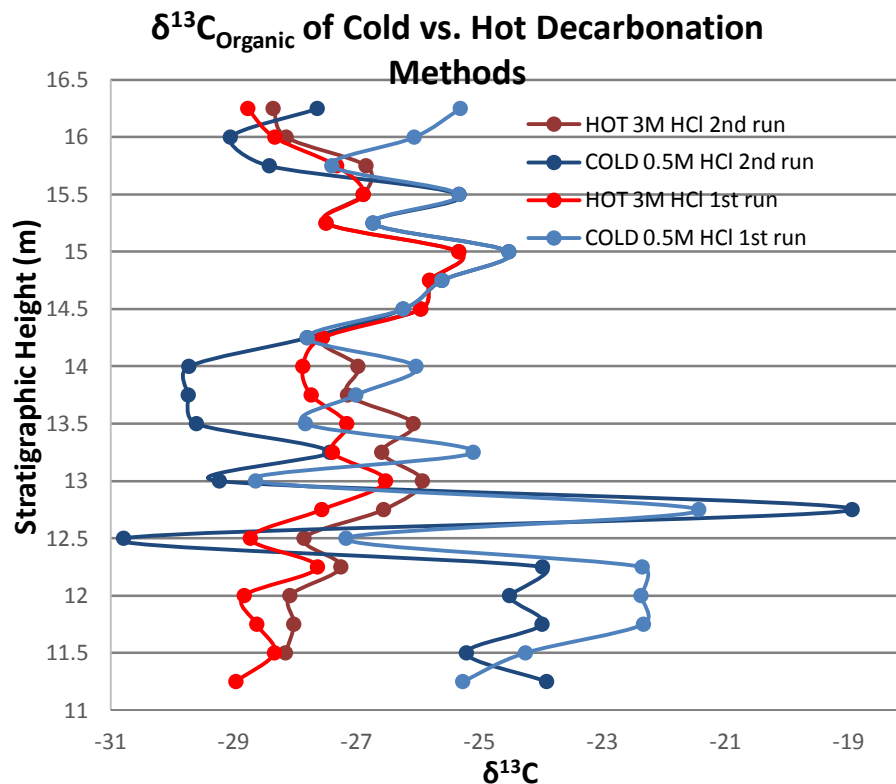
Figure 22. Various carbon-isotope chemostratigraphic profiles of upper 4.75 m of Lake Madsen section, derived from multiple IRMS runs of duplicate samples using hot or cold decarbonation methods. Shows variability in employing different acid concentrations and temperatures in decarbonation methods and variability in IRMS results of duplicate samples.

decarbonation reactions for both 0.5M "cold" and 3.0M "hot" HCl concentrations to generate a weight percent of dissolved solids. Comparisons were made for weight percent $CaCO_3$ dissolved in each sample at both temperatures and acid concentrations (Fig. 23). Weight percentages were almost identical for most samples except for the samples from the upper 1.75 meters of the section. These samples had dissolved weight percentages that varied by up to 15% and had no clear pattern of variability. Oddly, these samples were fairly consistent, although they varied somewhat, in IRMS run results while the samples that had consistent dissolved weight percentages were the ones that had more variable IRMS results. It is possible that human error could account for the differences in dissolved weight percentages, due to the action of pouring

Cold vs. Hot Wt. % CaCO$_3$ Lost
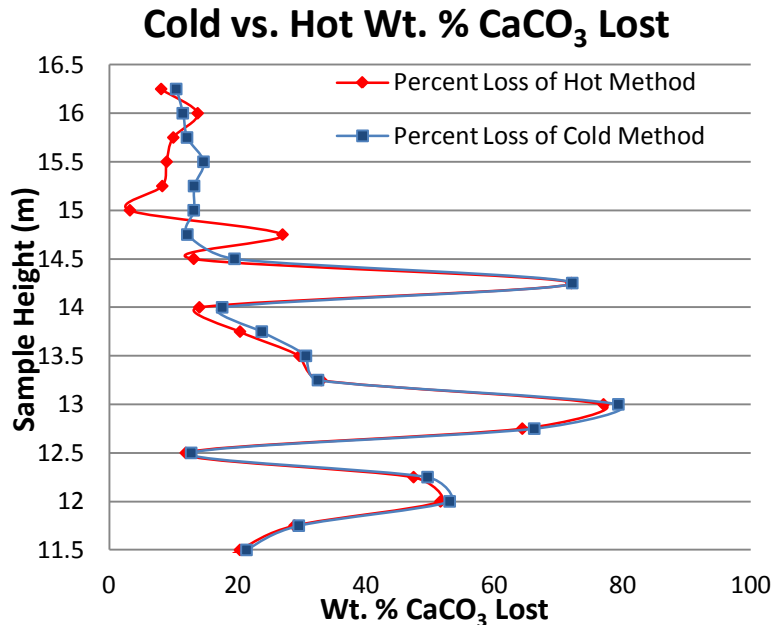
Figure 23. Dissolved weight percents of CaCO$_3$ removed for upper 4.75 meters of Lake Madsen section using both "cold" 0.5M and "hot" 3.0M HCl concentrations. Upper 1.75 meter samples vary but do not reflect variations in IRMS results.

off the supernatant acid during decarbonation. This can lead to sediment and associated organics being inadvertently poured off as well. X-ray diffraction of sediment samples could be used to determine if other carbonate species may be present within some of the samples and if they could be affecting the decarbonation reaction.

And still another possibility, although unlikely, may be that the IRMS calibration was off during initial sampling. Subsequent sample runs were made in duplicate and produced results that varied by ~2‰ but preserved the overall chemostratigraphic curve, displaying the range and accuracy of the IRMS. Another possible issue in replicating results is the low percentage of total organic carbon present in the sampled section. Being that it is a fluvial to lacustrine regime, recycling of organic material is a possibility, as nearby rocks are eroded and the organic material from those rocks is redeposited. Preservation of the isotopic composition of organic material derived from CMF time could become skewed by even a small contamination of older recycled organic material that preserves a different isotopic composition or has even possibly undergone

42

greater hydrocarbon fixation. Detection of recycled organic material could be done by examining vitrinite reflectance derived R_o values for organic matter in the sediment and calculating appropriate R_o values for the CMF and its members based on burial depth curves. These results suggest caution should be taken such as carefully cleaning the mortar and pestels, homogenizing the sediments completely, and mixing samples prior to weighing into tin cups when analyzing low total organic content samples. Nonetheless, values produced from various analyses are within 2σ, preserving the overall trend.

VII. Conclusions

A. $\delta^{13}C$ and $\delta^{18}O$ of Vertebrate Remains

Most vertebrate samples have $\delta^{18}O$ values of structural carbonate and structural phosphate that show similar trends observed by Iacumin et al., (1996) in modern vertebrate samples that possessed unaltered primary isotopic compositions falling on the equilibrium equation line, while some samples, namely RRM samples, have values that do not fall along the equilibrium line and likely have undergone some degree of diagenesis. Overall the observed diagenesis seems to be reasonably low and suggests the $\delta^{13}C_{CO3}$ from the samples can be used to accurately calculate MAP.

The estimated MAP values, derived from enamel $\delta^{13}C$, show a sharp decrease from the lower YCM to the upper YCM. This was likely related to an active period of thrusting, specifically the Canyon Range thrust, occurring at the time of deposition of the upper YCM creating a greater rain shadow effect over the depositional area. MAP values increase slightly during the emplacement of the RRM, which is surprising, considering the ample amounts of carbonate nodules and dolomite present within the RRM compared to the upper YCM. MAP increases

43

greatly in the MM as incursion of the Western Interior Seaway brings coastal moisture closer to the depositional area of the CMF.

To further prove the existence of an orographic rain shadow, comparisons should be made with isotopic data of similar aged deposits on the windward side of the SFTB. Deposits on the windward side should have considerably lighter $\delta^{13}C$ values preserved within the carbonate portion of vertebrate remains compared to those found in the CMF. $\delta^{18}O$ values of both carbonate and phosphate portions of tooth enamel should be considerably heavier with respect to values obtained from the CMF.

B.   Chemostratigraphy

Carbon isotope chemostratigraphy can be a useful tool in determining relative age of continental strata. Correlations between marine reference sections and Lake Madsen indicate a terrestrial manifestation of CIEs associated with OAE1a of the Aptian stage of the early Cretaceous. This constrains the relative depositional age of the Yellow Cat Member to 125-120 Ma or Barremian to Aptian. Despite these correlations, more work needs to be done to determine if these $\delta^{13}C$ chemostratigraphic correlations are accurate. Results were unable to be replicated for some bulk organic samples. Various explanations for this exist and need to be explored in greater detail.

Similar chemostratigrahic profiles are observed when comparing $\delta^{13}C$ of organic carbon and $\delta^{13}C$ and $\delta^{18}O$ of carbonate. This suggests that the isotopic concentrations are being controlled by atmospheric concentrations and should reflect global observations, making comparisons to similar aged sections around the world viable. Carbonate $\delta^{13}C$ and $\delta^{18}O$ show covariance suggesting deposition within a freshwater lake which coincides with lithological interpretations made for the upper YCM Lake Madsen section.

44

VIII.   References

Amiot, R., Lecuyer, C., Buffetaut, E., Escarguel, G., Fluteau, F., and Martineau, F., 2006. Oxygen isotopes from biogenic apatites suggest widespread endothermy in Cretaceous dinosaurs, Earth and Planetary Science Letters, v. 246, p. 41-54.

Amiot, R., Lecuyer, C., Escarguel, G., Billon-Bruyat, J.P., Buffetaut, E., Langlois, C., Martin, S., Martineau, F., and Mazin, J.M., 2007. Oxygen isotope fractionation between crocodilian phosphate and water: Palaeogeography, Palaeoclimatology, Palaeoecology, v. 243, p.412-420.

Aubrey, W.M., 1998. A newly discovered, widespread fluvial facies and unconformity marking the Upper Jurassic/Lower Cretaceous boundary, Colorado Plateau. *in* Carpenter, K., Chure, D., and Kirkland, J.I., eds., The Upper Jurassic Morrison Formation: An Interdisciplinary Study, Part I. Modern Geology, v. 22, p. 209-233.

Baars, D.L., and Doelling, H.H., 1987, Moab salt-intruded anticline, east-central Utah, in: S.S. Beus (ed.) Rocky Mountain section of the Geological Society of America, Centennial Field Guide, Volume 2, Geological Society of America, Boulder CO, p. 275-280.

Barrick, R.E., Fisher, A.L., and Showers, W.J., 1999. Oxygen isotopes from turtle bone: application for terrestrial paleoclimates? Palaios, v. 14, p. 186-191.

Bellanca, A., Erba, E., Rodolfo, N., Silva, I.P., Sprovieri, M., Tremolada, F., Verga, D., 2002. Palaeoceanographic significance of the Tethyan 'Livello Selli' (Early Aptian) from the Hybla Formation, northwestern Sicily, Palaeogeography, Palaeoclimatology, Palaeoecology, v. 185, p. 175-196.

Berner, R.A., 1990. Atmospheric carbon dioxide levels over Phanerozoic time. Science, v. 249, p. 1382-1386.

Britt, B.B., Burton, D., Greenhalgh, B.W., Christiansen, E., and Currie, D., 2007. Detrital zircon ages for the basal Cedar Mountain Formation (Early Cretaceous) near Moab, and Dinosaur National Monument, Utah [Abstract]. Geological Society of America, Abstracts with Programs, v. 39, p. 16.

Bryant, J.D., Froelich, P.N., 1995. A model of oxygen isotope fractionation in body water of large mammals. Geochem. Cosmochim. Acta. v. 59, p. 4523-4537.

Carpenter, K., and Kirkland, J.I., 1998. Review of Lower and Middle Cretaceous ankylosaurs from North America, in Lucas, S.G., Kirkland, J.I., and Estep, J.W., editors, Lower to Middle Cretaceous non-marine Cretaceous faunas: New Mexico Museum of Natural History and Science Bulletin 14, p. 249-270.

Cerling, T.E., 1999. Paleorecords of C_4 plants and ecosystems. In: Sage, R.F., Monson, R.K. (Eds.), C_4 Plant Biology. Academic Press, San Diego, p 445-472.

Cerling, T.E., Harris, J.M., 1999. Carbon isotope fractionation between diet and bioapatite in ungulate mammals and implications for ecological and paleoecological studies. Oecologia. v. 120, p. 347-363

Chenery, C.,Müldner, G., Evans, J., Eckardt, H., Lewis, M., 2010. Strontium and stable isotope evidence for diet and mobility in Roman Gloucester, UK. J. Arch. Sci. v. 37, p. 150–163.

Cifelli, R.L., Nydam, R.L., Gardner, J.D., Weil, A., Eaton, J.G., Kirkland, J.I., and Madsen, S.K., 1999. Medial Cretaceous vertebrates from the Cedar Mountain Formation, Emery County, the Mussentuchit local fauna, in Gillette, D., editor, Vertebrate paleontology in Utah: Utah Geological Survey Miscellaneous Publication 99-1, p. 219-242.

Currie, B.S., 2002. Structural configuration of the Early Cretaceous cordilleran foreland-basin system Sevier Thrust Belt, Utah and Colorado. Journal of Geology, v. 110, p. 697-718.

Dansgaard, W., 1964. Stable isotopes in precipitation. Tellus, v. 16, p. 436-468.

Dayvault, R.D., and Hatch, H.S., 2005. Cycads from the Upper Jurassic and Lower Cretaceous rocks of southeastern Utah: Rocks and Minerals, v. 80, no. 6, p. 412-432.

DeCelles, P.G., and Coogan, J.C., 2006. Regional structure and kinematic history of the Sevier fold-and-thrust belt, central Utah: Geological Society of America Bulletin, v. 118, p. 841-846, DOI 10.1130/B25759.1.

Derry, L.A., Kaufman, A.J., Jacobsen, S.B., 1992. Sedimentary cycling and environmental change in the Late Proterozoic: Evidence from stable and radiogenic isotopes. Geochemica et Cosmoschimica Acta, v. 56, p. 1317-1329.

Des Marais, D.J., Strauss, H., Summons, R.E., Hayes, J.M., 1992. Carbon isotope evidence for the stepwise oxidation of the Proterozoic environment. Nature, v. 359, p. 604-609.

Diefendorf, A.F., Mueller, K.E., Wing, S.L., Koch, P.L., Freeman, K.H., 2010. Global patterns in leaf ^{13}C discrimination and implications for studies of past and future climate. Proceedings of the National Academy of Sciences, v. 107, no. 13, p. 5738-5743.

Di Lucia, M., Trecalli, A., Mutti, M., and Parente, M., 2012. Bio-chemostratigraphy of the Barremian-Aptian shallow-water carbonates of the southern Apennines (Italy): pinpointing the OAE1a in a Tethyan carbonate platform. Solid Earth, v. 3, p. 1-28, DOI 10.5194/se-3-1-2012.

Dunkley-Jones, T., Ridgwell, A., Lunt, D.J., Maslin, M.A., Schmidt, D.N., Valdez, P.J., 2010. A Palaeogene perspective on climate sensitivity and methane hydrate instability. Philosophical Transactions of the Royal Society, v. A. 368, p. 2395-2415.

Ducea, M., 2001, The California arc: Thick granitic batholiths, eclogitic residues, lithospheric-scale thrusting, and magmatic fl are-ups: GSA Today, v. 11, p. 4–10, doi: 10.1130/1052-5173(2001)011<0004:TCATGB>2.0.CO;2.

Eagle, R.A., Tutken, T., Martin, T.S., Tripati, A.K., Fricke, H.C., Connely, M., Cifelli, R.L., and Eiler, J.M., 2011. Dinosaur body temperatures determined from isotopic (^{13}C-^{18}O) ordering in fossil biominerals. Science, v. 333, no. 6041, p. 443-445.

Ekart, D.D., Cerling, T.E., Montanez, I.P., Tanopr, N.J., 1999. A 400 million year carbon isotope record of pedogenic carbonate: Implications for paleoatmospheric carbon dioxide. American Journal of Science, v. 299, p. 805-827.

Epstein, S., Mayeda, T., 1953. Variations in the 18-O content of waters from natural sources. Geochim. Cosmochim Acta. v. 4, p. 213-224.

Erba, E., Channel, J.E.T., Claps, M., Jones, J., Larson, R., Opdyke, B., Premoli Silva, I., Riva, A., Salvini, G., Torricelli, S., 1999. Integrated stratigraphy of the Cismon Apticore (Southern Alps, Italy): a 'reference section' for the Barremian-Aptian interval at low latitudes. Journal of Foraminiferal Research, v. 29, p. 371-391.

Falkowski, P., 2003. Biogeochemistry of primary production in the sea. Treatise on Geochemistry. v. 8, p. 185-213.

Farquhar, G.D., Ehleringer, J.R., Hubick, K.T., 1989. Carbon isotope discrimination and photosynthesis. Annu. Rev. Plant Physiol. Plant Mol. Biol. v. 40, p. 503-537.

Fricke, H.C., Rogers, R.R., Backlund, R., Dwyer, C.N., Echt, S., 2008. Preservation of primary stable isotope signals in dinosaur remains, and environmental gradients of the Late Cretaceous of Montana and Alberta. Palaeogeography, Palaeoclimatology, Paleoecology v. 266, p. 13-27.

Garrison, J.R. Jr., Brinkman, D., Nichols, D.J., Layer, P., Burge, D., Thayn, D., 2007. A multidisciplinary study of the Lower Cretaceous Cedar Mountain Formation, Mussentuchit Wash, Utah: a determination of the paleoenviroment and paleoecology of the *Eolambia caroljonesa* dinosaur quarry. Cretaceous Research, v. 28, p. 461-494.

Greenhalgh, B.W., Britt, B.B., and Kowallis, B.J., 2006. New U-Pb age control for the lower Cedar Mountain Formation and an evaluation of the Morrison Formation/Cedar Mountain Formation boundary, Utah [abs.]: Geological Society of America Abstracts with Programs, v. 38, no. 6, p. 7.

Grocke, D.R., Hesselbo, S.P., Jenkyns, H.C., 1999. Carbon-isotope composition of Lower Cretaceous fossil wood: Ocean-atmosphere chemistry and relation to sea-level change: Geology; v. 27, no. 2, p. 155-158.

Hayes, J.M., Strauss, H., Kaufman, A.J., 1999. The abundance of ^{13}C in marine organic matter and isotopic fractionation in the global biogeochemical cycle of carbon during the past 800 Ma. Chemical Geology. v. 161, p. 103-125.

Herrle, J.O., Kubler, P., Friedrich, O., Erlenkeuser, H., and Hemleben, C., 2004. High-resolution carbon isotope records of the Aptian to Lower Albian from SE France and the Mazagan Plateau (DSDP Site 545): a stratigraphic tool for paleoceanographic and paleobiologic reconstruction. Earth and Planetary Science Letters, v. 218, p. 149-161.

Houghton, R.A., 2007. Balancing the global carbon budget. Annual Review of Earth and Planetary Sciences. v. 35, p. 313-347.

Iacumin, P., Bocherens, H., Mariotti, A., Longinelli, A., 1996. Oxygen isotope analyses of co-existing carbonate and phosphate in biogenic apatite; a way to monitor diagenetic alteration of bone phosphate?. Earth and Planetary Science Letters, v. 142, p. 1-6.

Jenkyns, H.C., 2003. Evidence for rapid climate change in the Mesozoic-Paleogene greenhouse world: Phil. Trans. R. Soc. Lond. A v. 361, p 1885-1916, DOI: 10.1098/rsta. 2003.1240.

Kirkland, J.I., Cifelli, R.L., Britt, B.B., Burge, D.L., DeCourten, F.L., Eaton, J.G., Parrish, J.M., 1999. Distribution of vertebrate faunas in the Cedar Mountain Formation, east-central Utah, in: D.D. Gillette (Ed.), Vertebrate Paleontology in Utah, Utah Geological Survey, Miscellaneous Publication, v. 99-1 (1999), p. 201–242.

Kirkland, J.I., 2005a. Utah's newly recognized dinosaur record from the Early Cretaceous Cedar Mountain Formation: Utah Geological Survey, Survey Notes, v. 33, no. 1, p. 1-5.

Kirkland, J.I., and Madsen, S.K., 2006. The lower Cretaceous Cedar Mountain Formation, eastern Utah: the view up an always interesting learning curve: 2007 Geological Society of America Rocky Mountain Section Annual Meeting, St. George, Utah.

Koch, P.L., 1997. The effects of sample treatment and diagenesis on the isotopic integrity of carbonate in biogenic hydroxylapatite, Journal of Archaeological Science v. 24, p. 417-429.

Koch, P.L., 1998. Isotopic reconstruction of past continental environments: Annu. Rev. Earth Planet. Sci. 1998. v. 26, p. 573–613.

Kohn, M.J., 1996. Predicting animal δ18O: accounting for diet and physiological adaptation: Geochimica et Cosmochimica Acta, v. 60, p. 4811-4829

Kohn, M.J., 2010. Carbon isotope compositions of terrestrial C3 plants as indicators of (paleo)ecology and (paleo)climate, PNAS, November 16, 2010, v. 107, no. 46, p. 19691–19695.

Kohn, M.J., Cerling, T.E., 2002. Stable isotope compositions of biological apatite. Rev. Mineral. Geochem. v. 48, p. 455-488.

Kohn, M.J., and Dettman, D.L., 2007. Paleoaltimetry from stable isotope compositions of fossils. Reviews in Mineralogy and Geochemistry, v. 66, p. 119-154.

Kowallis, B.J., Britt, B.B., Greenhalgh, B.W., and Sprinkel, D.A., 2007. A new U-Pb zircon age from an ash bed in the Brushy Basin Member of the Morrison Formation near Hanksville, UT [Abstract]. Geological Society of America, Abstracts with Programs, v. 39, p. 9.

Kump, L.R., Arthur, M.A., 1999. Interpreting carbon-isotope excursions: Carbonates and organic matter. Chemical Geology. v. 161, p. 181-198.

Leng, M.J., Lamb, A.L., Heaton, T.H., Marshall, J.D., Wolfe, B.B., Jones, M.D., Arrowsmith, C., 2006. Isotopes in lake sediments In: Leng, M.J. (Ed.), Isotopes in Palaeoenvironmental Research. Springer, Netherlands, p. 147-184.

Longinelli, A., 1984. Oxygen isotopes in mammal bone phosphate: a new tool for paleohydrological and paleoclimatological research? Geochem. Cosmochim. Acta. v. 48, p. 385-390.

Ludvigson, G. A., Joeckel, R. M., Gonzalez, L. A., Gulbranson, E. L., Rasbury, E. T., Hunt, G. J., Kirkland, J. I., and Madsen, S., 2010a. Correlation of Aptian-Albian carbon isotope excursions in continental strata of the Cretaceous foreland basin, eastern Utah, U.S.A.: Journal of Sedimentary Research, 2010, v. 80, p. 955–974 Research Article DOI: 10.2110/jsr.2010.086.

Luz, B., Kolodny, Y., 1985. Oxygen isotope variations in phosphates of biogenic apatites, IV: Mammal teeth and bones. Earth Planet. Sci. Lett. v. 75, p. 29-36.

Lynch-Stieglitz, J., 2003. Tracers of past ocean circulation. Treatise on Geochemistry. v. 6, p. 433-451.

Maslin, M.A., Swann, G.E.A., 2005. Isotopes in marine sediments. In: Leng, M.J. (Ed.), Isotopes in Paleoenviromental Research. Springer, Dordrecht, Netherlands, p. 227-290.

Maslin, M.A., Thomas, E., 2003. Balancing the deglacial global carbon budget: The hydrate factor. Quaternary Science Reviews. v. 22, p. 1729-1736.

Mengatti, A.P., Weissert, H., Brown, R.S., Tyson, R.V., Farrimond, P., Strasser, A. and Caron, M., 1999. High-resolution $\delta^{13}C$ stratigraphy through the early Aptian "Livello Selli" of the Alpine Tethys, Paleoceanography, v. 13, no. 5, p. 530-545.

O'Leary, M.H., 1998. Carbon isotopes in photosynthesis. Bioscience v. 38, p. 328-336.

O'Leary, M.H., Mahavan, S., Paneth, P., 1992. Physical and chemical basis of carbon isotope fractionation in plants. Plant Cell Environ. v. 15, p. 1099-1104.

O'Neil, J.R., Clayton, R.N., and Mayeda, T.K., 1969. Oxygen isotope fractionation in divalent metal carbonates. Journal of Chemical Physics, v. 51, p. 5547-5558.

Passey, B.H., Robinson, T.F., Ayliffe, L.K., Cerling, T.E., Sponheimer, M., Dearing, M.D., Roeder, B.L., Ehlinger, J.R., 2005. Carbon isotope fractionation between diet, breath CO_2, and bioapatite in different mammals. J. Archaeol. Sci. v. 32, p. 1459-1470

Poulsen, C., David, P., and White, T.S., 2007. General circulation model simulation of the $\delta^{18}O$ content of continental precipitation in the middle Cretaceous: a model-proxy comparison. Geology, v. 35, p. 199-202.

Ravizza, G.E., Zachos, J.C., 2003. Records of Cenozoic Ocean Chemistry. Treatise on Geochemistry (Elsevier) v. 6, p. 551-581.

Robinson, S.A., Hesselbo, S.P., 2004. Fossil-wood carbon-isotope stratigraphy of the non-marine Wealden Group (Lower Cretaceous, southern England). Journal of the Geological Society. v. 161, p. 133-145.

Rozanski, K., Araguas-Araguas, L., Gonfiantini, R., 1993. Isotopic patterns in modern global precipitation. In: Swart, P.K., Lohmann, K.C., McKenzie, J., Savin, S. (Eds.), Climate Change in the Continental Isotopic Records. American Geophysical Union, Washington, D.C., p. 1-36.

Saltzman, M.R., Thomas, E., 2012. Carbon Isotope Stratigraphy, Chapter 11, The Geologic Time Scale 2012. DOI: 10.1016/B978-0-444-59425-9.00011-1, p. 207-232.

Sarmiento, J.L., Gruber, N., 2006. Ocean Biogeochemical Dynamics. Princeton University Press, Princeton, NJ (USA), p. 503.

Shackleton, N.J., Hall, M.A., 1984. Carbon isotope data from Leg 74 sediments. Initial Reports of Deep Sea Drilling Project 74, p. 613-619.

Shackleton, N.J., 1987. The carbon isotope record of the Cenozoic: History of organic carbon burial and of oxygen in the ocean and atmosphere. In: Brooks, J., Fleet, A.J., (Eds.), Marine Petroleum Source Rocks, Geological Society Special Publication 26: London, p. 423-434.

Spicer, R.A., and Corfield, R.M., 1992. A review of terrestrial and marine climates in the Cretaceous with implications for modeling the "Greenhouse Earth". Geological Magazine, v. 2, p. 169-180.

Stikes, M.W., 2006. Fluvial facies and architecture of the Poison Strip Sandstone, Lower Cretaceous Cedar Mountain Formation, Grand County, Utah: Utah Geological Survey Miscellaneous Publication, v. 06-2, p. 84, CD-ROM.

Suarez, C.A., Gonzalez, L.A., Ludvigson, G.A., Cifelli, R.L., and Treman, E., 2012. Water utilization of the Cretaceous Mussentuchit Member local vertebrate fauna, Cedar Mountain Formation, Utah, U.S.A.: using oxygen isotopic composition of phosphate. Palaeogeography, Palaeoclimatology, Palaecology, v. 313-314, p. 78-92.

Suarez, C.A., Gonzalez, L.A., Ludvigson, G.A., Kirkland, J. I., Cifelli, R.L., and Kohn, M.J., 2014. Isotopic insights into the paleohydrologic record in a Cretaceous foreland basin. Journal of Sedimentary Research, v. 84, p. 975-987.

Suarez, M.B., Gonzalez, L.A., Ludvigson, G. A., 2011. Quantification of a greenhouse hydrologic cycle from equatorial to polar latitudes: The mid-Cretaceous water bearer revisited. Palaeogeography, Palaeoclimatology, Paleoecology 307, 2011, p. 301-312.

Suarez, M.B., Ludvigson, G.A., Gonzalez, L.A., Al-Suwaidi, A.H., You, H., 2013. Stable isotope chemostratigraphy in lacustrine strata of the Xiagou Formation, Gansu Province, NW China. Geological Society, London, Special Publications, v. 382, p. 143-154.

Sundquist, E.T., Visser, K., 2004. The Geologic History of the Carbon Cycle. Treatise on Geochemistry. v. 8, p. 425-472.

Tarduno, J.A., Sliter, W.V., Kroenke, L., Leckie, M., Mayer, H., Mahoney, J.J., Musgrave, R., Storey, M., Winterer, E.L., 1991. Rapid formation of Ontong Java Plateau by Aptian mantle plume volcanism. Science, v. 254, p. 399-403.

Taylor, B., 2006. The single largest oceanic plateau: Ontong Java–Manihiki–Hikurangi. Earth and Planetary Science Letters, v. 241, p. 372-380.

Tidwell, W.D., 1996. Cretaceous flora of east-central Utah and western Colorado – A review, in Herendeeen, P.S., Johnson, K., Tidwell, W.D., and Ash, S.R., editors, Guidebook for Paleozoic, Mesozoic, and Cenozoic excursion of Utah and Colorado: The Fifth Annual Paleobotanical Conference, p. 57-72.

Tieszen, L.L., 1991. Natural variations in carbon isotope values of plants: implications for archaeology, ecology, and paleoecology. J. Archaeol. Sci. v. 20, p. 227-248.

Tschudy, R.H., Tschudy, B.D., Craig, L.C., 1984. Palynological evaluation of Cedar Mountain and Burro Canyon Formations, Colorado Plateau. US Geological Survey, Professional Paper 1281, v. 24, p. 9.

Ufnar, D.F., Gonzalez, L.A., Ludvigson, G.A., Brenner, R. L., and Witzkf, B.J., 2004. Evidence for increased latent heat transport during the Cretaceous (Albian) greenhouse warming. Geology, v. 32, p. 1049-1052.

Wang, Y. and Cerling, T.E., 1994. A model of fossil tooth and bone diagenesis: implications for paleodiet reconstruction from stable isotopes. Palaeogeography, Palaeoclimatology, Palaeoecology, v. 107, p. 281-289.

White, T., Gonzalez, L.A., Ludvigson, G.A., and Poulsen, C., 2001. Middle Cretaceous greenhouse hydrologic cycle of North America. Geology, v. 29, p. 363-366.

Wolfe, J.A., and Upchurch, G., 1987. North American nonmarine climates and vegetation during the Late Cretaceous. Palaeogeography, Palaeoclimatology, Palaeoecology, v. 61, p. 33-77.

van der Merwe, N.J., Medina, E., 1991. The canopy effect, carbon isotope ratios and foodwebs in Amazonia. J. Archaeol. Sci. v. 18, p. 249-259.

Young, R.G., 1960. Dakota Group of Colorado Plateau. American Association of Petroleum Geologists Bulletin, v. 44, p. 158-194.

Appendix A

Sample	Stratigraphic Height (m)	$\delta^{13}C_{organic}$ vs. VPDB (Run #1 - 0.5M HCl @ 25°C)	$\delta^{13}C_{organic}$ vs. VPDB (Run #2 - 0.5M HCl @ 25°C)	$\delta^{13}C_{organic}$ vs. VPDB (Run #3 - 3.0M HCl @ 25°C)	$\delta^{13}C_{organic}$ vs. VPDB (Run #4 - 3.0M HCl @ 60°C)	$\delta^{13}C_{organic}$ vs. VPDB (Run #5 - 3.0M HCl @ 60°C)	$\delta^{13}C_{organic}$ vs. VPDB (Run #6 - 3.0M HCl @ 60°C)	Total standard deviation of $\delta^{13}C_{organic}$	$\delta^{13}C_{CO3}$ vs. VPDB	Standard Deviation of $\delta^{13}C_{CO3}$	$\delta^{18}O_{CO3}$ vs. VPDB	Standard Deviation of $\delta^{18}O_{CO3}$
LMDS - contact	0.00	-24.34	NA	NA	NA	NA	NA	0.42	NA	NA	NA	NA
LMDS - 0	0.25	-26.12	NA	NA	NA	NA	NA	0.41	NA	NA	NA	NA
LMDS - 1	0.50	-23.98	NA	NA	NA	NA	NA	0.51	NA	NA	NA	NA
LMDS - 2	0.75	-23.68	NA	NA	NA	NA	NA	0.54	NA	NA	NA	NA
LMDS - 3	1.00	-24.07	NA	NA	NA	NA	NA	0.55	NA	NA	NA	NA
LMDS - 4	1.25	-24.03	NA	NA	NA	NA	NA	0.55	NA	NA	NA	NA
LMDS - 5	1.50	-24.45	NA	NA	NA	NA	NA	0.55	NA	NA	NA	NA
LMDS - 6	1.75	-23.33	NA	NA	NA	NA	NA	0.53	NA	NA	NA	NA
LMDS - 7	2.00	-23.81	NA	NA	NA	NA	NA	0.55	NA	NA	NA	NA
LMDS - 8	2.25	-24.14	NA	NA	NA	NA	NA	0.54	NA	NA	NA	NA
LMDS - 9	2.50	-23.56	NA	NA	NA	NA	NA	0.57	NA	NA	NA	NA
LMDS - 10	2.75	-24.11	NA	NA	NA	NA	NA	0.57	NA	NA	NA	NA
LMDS - 11	3.00	-24.01	NA	NA	NA	NA	NA	0.57	NA	NA	NA	NA
LMDS - 12	3.25	-23.63	NA	NA	NA	NA	NA	0.56	NA	NA	NA	NA
LMDS - 13	3.50	-23.92	NA	NA	NA	NA	NA	0.57	NA	NA	NA	NA
LMDS - 14	3.75	-23.80	NA	NA	NA	NA	NA	0.55	NA	NA	NA	NA
LMDS - 15	4.00	-23.98	NA	NA	NA	NA	NA	0.55	NA	NA	NA	NA
LMDS - 16	4.25	-22.72	NA	NA	NA	NA	NA	0.55	NA	NA	NA	NA
LMDS - 17	4.50	-23.72	NA	NA	NA	NA	NA	0.53	NA	NA	NA	NA
LMDS - 18	4.75	-24.57	NA	NA	NA	NA	NA	0.52	NA	NA	NA	NA
LMDS - 19	5.00	-24.88	NA	NA	NA	NA	NA	0.54	NA	NA	NA	NA
LMDS - 20	5.25	-24.68	NA	NA	NA	NA	NA	0.56	NA	NA	NA	NA
LMDS - 21	5.50	-24.80	NA	NA	NA	NA	NA	0.53	NA	NA	NA	NA
LMDS - 22	5.75	-24.70	NA	NA	NA	NA	NA	0.56	NA	NA	NA	NA
LMDS - 23	6.00	-24.83	NA	NA	NA	NA	NA	0.55	NA	NA	NA	NA
LMDS - 24	6.25	-24.65	NA	NA	NA	NA	NA	0.53	NA	NA	NA	NA
LMDS - 25	6.50	-24.39	NA	NA	NA	NA	NA	0.54	NA	NA	NA	NA
LMDS - 26	6.75	-24.56	NA	NA	NA	NA	NA	0.53	NA	NA	NA	NA
LMDS - 27	7.00	-24.50	NA	NA	NA	NA	NA	0.31	NA	NA	NA	NA
LMDS - 28	7.25	-24.20	NA	NA	NA	NA	NA	0.36	NA	NA	NA	NA
LMDS - 29	7.50	-24.15	NA	NA	NA	NA	NA	0.49	NA	NA	NA	NA
LMDS - 30	7.75	-24.99	NA	NA	NA	NA	NA	NA	-5.59	0.05	-8.03	0.08
LMDS - 31	8.00	-26.76	NA	NA	NA	NA	NA	NA	-5.84	0.05	-8.38	0.13
LMDS - 32	8.25	-25.1	NA	NA	NA	NA	NA	NA	-4.42	0.09	-8.24	0.11
LMDS - 33	8.50	-24.74	NA	NA	NA	NA	NA	NA	-4.40	0.05	-7.90	0.09
LMDS - 34	8.75	-25.14	NA	NA	NA	NA	NA	NA	-4.45	0.04	-7.92	0.07
LMDS - 35	9.00	-24.98	NA	NA	NA	NA	NA	NA	-5.70	0.03	-8.95	0.11
LMDS - 36	9.25	-24.89	NA	NA	NA	NA	NA	NA	-6.68	0.06	-9.64	0.36
LMDS - 37	9.50	-24.95	NA	NA	NA	NA	NA	NA	-7.30	0.25	-10.02	0.50
LMDS - 38	9.75	-25.15	NA	NA	NA	NA	NA	NA	-7.46	0.39	-10.57	0.82
LMDS - 39	10.00	-25.18	NA	NA	NA	NA	NA	NA	-6.75	0.07	-9.10	0.11
LMDS - 40	10.25	-25.82	NA	NA	NA	NA	NA	NA	-3.75	0.05	-9.31	0.03
LMDS - 41	10.50	-25.99	NA	NA	NA	NA	NA	NA	-4.49	0.06	-8.87	0.11
LMDS - 42	10.75	-24.54	NA	NA	NA	NA	NA	NA	-5.67	0.02	-9.43	0.04
LMDS - 43	11.00	-25.25	NA	NA	NA	NA	NA	NA	-5.06	0.05	-8.29	0.07
LMDS - 44	11.25	-25.27	NA	NA	NA	NA	NA	NA	-6.03	0.10	-8.64	0.15
LMDS - 45	11.50	-24.25	-25.21	-24.52	-28.33	-28.15	-25.33	1.81	-5.65	0.07	-8.48	0.15
LMDS - 46	11.75	-22.33	-23.98	-23.70	-28.62	-28.02	-25.00	2.51	-5.44	0.02	-8.26	0.06
LMDS - 47	12.00	-22.37	-24.51	-23.84	-28.83	-28.08	-24.73	2.52	-5.20	0.06	-7.88	0.09
LMDS - 48	12.25	-22.35	-23.97	-22.47	-27.63	-27.25	-25.13	2.29	-5.26	0.04	-7.96	0.06
LMDS - 49	12.50	-27.17	-30.79	-24.20	-28.73	-27.85	-24.60	2.50	-6.24	0.11	-9.91	0.14
LMDS - 50	12.75	-21.43	-18.93	-23.32	-27.56	-26.56	-24.08	3.20	-4.74	0.05	-7.72	0.04
LMDS - 51	13.00	-28.49	-29.23	-23.59	-26.53	-25.93	-23.62	2.37	-4.79	0.13	-7.81	0.12
LMDS - 52	13.25	-25.1	-27.43	-24.13	-27.39	-26.59	-24.80	1.42	-6.07	0.09	-9.71	0.05
LMDS - 53	13.50	-27.83	-29.60	-22.57	-27.16	-26.07	-24.37	2.52	-5.25	0.04	-8.86	0.05
LMDS - 54	13.75	-27.01	-29.74	-22.19	-27.74	-27.14	-23.64	2.79	-6.24	0.09	-8.79	0.16
LMDS - 55	14.00	-26.03	-29.73	-24.18	-27.87	-26.98	-23.90	2.23	-5.33	0.13	-8.11	0.11
LMDS - 56	14.25	-27.8	-27.8	-23.88	-27.55	-27.55	-24.38	1.84	-4.44	0.08	-7.98	0.06
LMDS - 57	14.50	-26.24	-26.24	-23.11	-25.95	-25.95	-23.38	1.48	-5.94	0.08	-8.55	0.05
LMDS - 58	14.75	-25.61	-25.61	-24.07	-25.81	-25.81	-23.79	0.93	-6.20	0.22	-8.80	0.31
LMDS - 59	15.00	-24.52	-24.52	-24.09	-25.33	-25.33	-23.93	0.60	-6.06	0.07	-9.40	0.20
LMDS - 60	15.25	-26.73	-26.73	-24.13	-27.49	-27.49	-24.96	1.39	-5.97	0.18	-9.78	0.29
LMDS - 61	15.50	-25.33	-25.33	-23.89	-26.89	-26.89	-24.29	1.26	-4.86	0.09	-8.68	0.24
LMDS - 62	15.75	-27.4	-28.42	-23.69	-27.32	-26.84	-23.84	2.00	-4.56	NA	-8.75	NA
LMDS - 63	16.00	-26.06	-29.05	-23.52	-28.33	-28.14	-24.84	2.20	-5.04	NA	-8.63	NA
LMDS - 64	16.25	-25.31	-27.64	-23.54	-28.77	-28.36	-24.32	2.22	-4.64	NA	-9.16	NA

Table 1: Data compilation of Lake Madsen Discovery Site (LMDS) chemostratigraphic samples and analyses.

sample	δ¹³C vs. VPDB	stdev δ¹³C	δ¹⁸O$_{CO3}$ vs. VSMOW	stdev δ¹⁸O$_{CO3}$	δ¹⁸O$_{PO4}$ vs. VSMOW	location	member	taxa
OMNH-32104-c6	-6.22	0.06	20.8	0.48	15.86	WS27(v868)	Mussentuchit	Hadrosaur
OMNH-32104-c5	-6.11	0.08	23.08	0.09	17.23	WS27(v868)	Mussentuchit	Hadrosaur
OMNH-26496-h1	-3.42	0.3	26.15	0.4	17.47	WS10(V695)	Mussentuchit	Ornithischia
OMNH-29990-ws9	-6.04	0.12	24.6	0.1	16.23	WS9	Mussentuchit	Ornithischia
OMNH-26496-h2-b	-2.87	0.06	22.7	0.09	16.94	WS10(V695)	Mussentuchit	Ornithischia
OMNH-26251-c2	-5.88	0.15	23.26	0.09	15.35	V239(sc1)	Mussentuchit	Hadrosaur
OMNH-61018-f1	-6.8	0.08	21.05	0.83	17.83	WS27(v868)	Mussentuchit	Lepisosteidea
OMNH-61018-h1	-6.86	0.12	21.06	0.07	16.32	WS27(v868)	Mussentuchit	Lepisosteidea
OMNH-29945-c2	-1.42	0.03	22.75	0.25	13.04	WS9	Mussentuchit	Osteichtheyes
OMNH-29945-c1	-3.49	0.09	23.34	0.08	14.70	WS9	Mussentuchit	Osteichtheyes
OMNH-29945-b1	-3.36	0.04	22.36	0.09	14.55	WS9	Mussentuchit	Osteichtheyes
OMNH-29945-b2	-2.86	0.05	22.2	0.08	14.23	WS9	Mussentuchit	Osteichtheyes
OMNH-28016-j	-3.02	0.05	21.68	0.47	16.01	V794(WS13)	Mussentuchit	Osteichtheyes
OMNH-28016-c-2	-4.44	0.13	20.33	0.46	13.30	WS13	Mussentuchit	Osteichtheyes
OMNH-25544-c3	-8.13	0.35	20.17	0.47	16.13	V235(WS4)	Mussentuchit	Crocodilia
OMNH-60901-a-6	-7.86	0.2	21.75	0.13	16.77	V868 (WS27)	Mussentuchit	Chelonia
CEUM-31948-11	-7.25	0.09	26.71	0.16	21.23	PR2	Ruby Ranch	Brachiosaur
CEUM-31948-9	-7.15	0.04	26.58	0.17	21.02	PR2	Ruby Ranch	Brachiosaur
DMNH-55492-c2	-7.02	0.11	27.08	0.45	15.61	PR2	Ruby Ranch	Iguanodontid
CEUM-31232-4	-7.5	0.23	29.53	0.15	23.09	PR2	Ruby Ranch	Acrocanthosaurus
CEUM-35842-6	-6.01	0.07	27.94	0.21	15.25	PR2	Ruby Ranch	Acrocanthosaurus
CEUM-35798-4	-7.93	0.11	28.61	0.17	17.02	PR2	Ruby Ranch	Crocodilia
No ID turtle-2	-6.92	0.06	22.69	0.24	14.29	PR2	Ruby Ranch	Chelonia
CEUM-11736-g	-5.89	0.12	26.41	0.33	15.61	PR3	Ruby Ranch	Chelonia
CEUM-12843-4	-6.65	0.12	30.67	0.36	14.75	PR4	Ruby Ranch	Naomichelys
CEUM-12843-6	-6.05	0.14	29.71	0.47	14.80	PR5	Ruby Ranch	Naomichelys
BYUVP-18171-2	-6.41	0.27	26.89	0.53	22.86	DWDQ	u-Yellow Cat	Sauropod
BYUVP-18171-3	-6.11	0.20	27.57	0.49	22.62	DWDQ	u-Yellow Cat	Sauropod
BYUVP-18171-4	-6.52	0.26	27.06	0.36	22.01	DWDQ	u-Yellow Cat	Sauropod
BYUVP-18185-1	-4.73	0.09	23.02	0.36	17.26	DWDQ	u-Yellow Cat	Sauropod
BYUVP-18185-2	-4.39	0.18	22.94	0.16	16.75	DWDQ	u-Yellow Cat	Sauropod
BYUVP-18185-4	-4.21	0.16	22.93	0.35	17.15	DWDQ	u-Yellow Cat	Sauropod
DB-Brach3-3	-8.42	0.25	23.86	0.60	17.11	Doelling's Bowl	l-Yellow Cat	Brachiosaur
DB-Brach-32	-9.07	0.17	27.34	0.22	?	Doelling's Bowl	l-Yellow Cat	Brachiosaur
DB-Brach-31	-8.68	0.17	27.13	0.26	?	Doelling's Bowl	l-Yellow Cat	Brachiosaur
BYUVP-7510-2	-5.94	0.27	27.25	0.33	?	DWDQ	u-Yellow Cat	Utahraptor
BYUVP-7510-3	-5.64	0.14	27.26	0.21	?	DWDQ	u-Yellow Cat	Utahraptor
BYUVP-7510-4	-5.40	0.16	27.74	0.31	?	DWDQ	u-Yellow Cat	Utahraptor
BYUVP-18104-2	-6.33	0.27	21.30	0.27	16.80	DWDQ	u-Yellow Cat	Utahraptor
BYUVP-18104-3	-6.20	0.17	20.91	0.52	16.72	DWDQ	u-Yellow Cat	Utahraptor
BYUVP-18104-4	-6.11	0.22	22.51	0.18	18.26	DWDQ	u-Yellow Cat	Utahraptor
BYUVP-14452-1	-6.79	0.20	21.34	0.28	17.68	DWDQ	u-Yellow Cat	Utahraptor
BYUVP-14452-2	-6.67	0.09	21.48	0.15	17.67	DWDQ	u-Yellow Cat	Utahraptor
BYUVP-14452-3	-6.80	0.18	22.15	0.58	17.98	DWDQ	u-Yellow Cat	Utahraptor
BYUVP-18099-1	-6.22	0.41	21.18	0.39	17.77	DWDQ	u-Yellow Cat	Utahraptor
BYUVP-18099-2	-6.72	0.23	20.34	0.94	17.93	DWDQ	u-Yellow Cat	Utahraptor
BYUVP-18099-3	-6.40	0.24	22.59	0.33	18.97	DWDQ	u-Yellow Cat	Utahraptor
UMNH-VP-16867-1	-6.46	0.20	19.15	0.45	13.3	AS	Yellow Cat	Crocodilia
UMNH-VP-16867-2	-6.53	0.29	19.79	0.20	13.3	AS	Yellow Cat	Crocodilia
UMNH-VP-16867-3	-6.58	0.24	20.12	0.62	12.5	AS	Yellow Cat	Crocodilia
UMNH-VP-16867-4	-6.44	0.26	19.83	0.34	14.1	AS	Yellow Cat	Crocodilia
UMNH-VP-16867-5	-6.68	0.10	19.62	0.28	13.7	AS	Yellow Cat	Crocodilia
UMNH-VP-16867-6	-6.36	0.25	19.77	0.36	14.1	AS	Yellow Cat	Crocodilia
UMNH-VP-16867-7	-6.19	0.24	19.45	0.28	13.3	AS	Yellow Cat	Crocodilia
UMNH-VP-16867-8	-6.26	0.23	19.49	0.49	14.1	AS	Yellow Cat	Crocodilia
UMNH-VP-16867-9	-6.33	0.10	19.29	0.37	13	AS	Yellow Cat	Crocodilia
UMNH-VP-16867-10	-6.25	0.20	19.23	0.36	14	AS	Yellow Cat	Crocodilia
UMNH-VP-16867-11	-6.24	0.35	19.58	0.57	14.1	AS	Yellow Cat	Crocodilia
UMNH-VP-16867-12	-6.03	0.12	19.53	0.27	14.3	AS	Yellow Cat	Crocodilia
DB-Croc1-4	-7.12	0.12	24.78	0.26	18.59	Doelling's Bowl	l-Yellow Cat	Crocodilia
DB-Croc1-5	-7.38	0.29	24.56	0.28	18.78	Doelling's Bowl	l-Yellow Cat	Crocodilia

Table 2. Results for isotope analysis of vertebrate samples of the Cedar Mountain Formation.